Chakraborty *et al.*
*Journal of Materials Science: Materials Theory* (2024) 8:3
https://doi.org/10.1186/s41313-024-00054-w

Journal of Materials Science: Materials Theory

RESEARCH Open Access

# Role of interfaces on the mechanical response of accumulative roll bonded nanometallic laminates investigated via dislocation dynamics simulations

Aritra Chakraborty[1], Aaron A. Kohnert[1], Abigail Hunter[2] and Laurent Capolungo[1*]

*Correspondence: laurent@lanl.gov

[1] Material Science and Technology division Los Alamos National Laboratory, Los Alamos 87544, NM, USA
[2] X Computational Physics division, Los Alamos National Laboratory, Los Alamos 87544, NM, USA

## Abstract

Unraveling the effects of continuous dislocation interactions with interfaces, particularly at the nanometer length scales, is key to a broader understanding of plasticity, to material design and to material certification. To this end, this work proposes a novel discrete dislocation dynamics-based model for dislocation interface interactions tracking the fate of residual dislocation on interfaces. This new approach is used to predict the impact of dislocation/interface reactions on the overall mechanical behavior of accumulative roll bonded nanometallic laminates. The framework considers the dynamic evolution of the interface concurrent with a large network of dislocations, thus, accounting for the local short and long range effects of the dislocations under the external boundary conditions. Specifically, this study focuses on two-phase Fe/Cu nanometallic laminates, and investigates the role of the underlying elastic and plastic contrast of the Fe and the Cu layers on the composite response of the material. Moreover, the role of initial microstructures, resulting from processing is also investigated. Subsequently, the model is used to examine the effect of layer thickness and interface orientation relationship on the residual stresses of the relaxed microstructure. The associated mechanical response of these laminates are compared when loaded under normal direction compression, as well as shear compression. Finally, this work predicts a dominant effect of the layer thickness, as compared to the interface orientation relationship, on the macroscopic response and on the residual stresses of these nanolaminates, while the local dislocation transmission propensity through the interface is significantly influenced by the corresponding orientation relationship.

**Keywords:** Dislocation-interface effects, Nanoscale plasticity, Slip transmission, Multiphase nanolaminates

## Introduction

Nanometallic laminates (NMLs) have received significant attention over the past few decades due to their good mechanical properties (e.g., hardness and flow stress) (Nizolek et al. 2015, 2016), thermal stability (Misra et al. 2004; Carpenter et al. 2013;

Zheng et al. 2013) and resistance to radiation damage (Demkowicz et al. 2008, 2010). NMLs also serve as model materials to study deformation mechanisms (e.g. dislocation/interface interactions) at the nanoscale (Misra and Hoagland 2007; Beyerlein et al. 2012; Cao et al. 2019).

Typically these metallic nanolaminates are synthesized via physical vapor deposition (PVD) (Mara et al. 2008; Josell et al. 1998; Menezes and Anderson 1990; Tench and White 1991), where two desired materials are alternatively deposited until the desired thickness is reached. Naturally, the specimens dimensions reachable with PVD render both mechanical testing (Nizolek et al. 2016) and overall technology deployment challenging. An alternative, consists of using accumulative roll bonding (ARB) to process NMLs in bulk form with layer thicknesses ranging from mm to nm scales (Yang et al. 2010; Min et al. 2006; Eizadjou et al. 2008; Ghalandari and Moshksar 2010; Wu et al. 2010; Beyerlein et al. 2013; Carpenter et al. 2014). Clearly the initial microstructure of NMLs processed by PVD and by ARB will differ (texture, residual stresses, dislocation content, interface morphology, etc.).

Overall, the structure, spacing and morphology of hetero-interfaces present in NMLs as well as the defect content will condition the plastic response and failure of the composite (Wang and Misra 2011; Beyerlein et al. 2013; Zhang et al. 2017; Radchenko et al. 2018; Misra et al. 2005; Hoagland et al. 2006; Meyers et al. 2006; Misra et al. 2008; Wang and Misra 2011).

At low layer thicknesses of $\approx$ 2-5 nm, plastic flow is mediated by dislocation cutting across the interface;while confined layer slip (CLS) becomes the dominant mechanism at larger layer thicknesses up to 100 nm. Note that direct observation of CLS was seen in NMLs with $\approx$ 30 nm thickness (Li et al. 2012). Finally, a more bulk type deformation where the formation of dislocation pile-ups dominates at even higher layer thicknesses (Pande et al. 1993; Anderson and Li 1995; Friedman and Chrzan 1998; Anderson et al. 1999; Misra and Kung 2001; Misra and Hoagland 2005, 2007).

Studies have thus focused on understanding and predicting single slip dislocation behavior, CLS, where threading dislocations are restricted to glide in their own layers with the intent to comprehend size effects, internal stress developments and potential plastic anisotropy in the response. In parallel, focus was also placed on studying slip transmission and/or dislocation emission from hetero-interfaces, especially at the continuum scale. We note that recent experimental studies have clearly demonstrated the fate of dislocations at heterointerfaces (i.e., accumulation of dislocations at the heterointerface, formation of geometrically necessary dislocation structures near interfaces, slip transmission) plays a critical role in controlling the onset of kink band formation during loading normal to the rolling direction (Zhang et al. 2022, 2023), the fatigue response of the material (Kümmel et al. 2019) and the overall degree to which the dissimilar materials can co-deform (Pohl et al. 2023).

Note that, beyond the consideration of NMLs, the body of literature dedicated to dislocation/interface reactions and transmission events is vast. Indeed, approaches have ranged from considering geometric configurations only (Robertson et al. 1989; Werner and Prantl 1990; Misra et al. 2002; Lim and Raj 1985; Livingston and Chalmers 1957) to atomistic simulations (Wang et al. 2008; Chu et al. 2013; Hoagland et al. 2004; Akasheh et al. 2007; Zbib et al. 2011) to meso-scale continuum mechanical models (Koehler 1970;

Pacheco and Mura 1969; Mayeur et al. 2013; Shehadeh et al. 2007; Mourad and Garikipati 2006; Wang et al. 2014; Shao et al. 2018). Most modeling efforts concerning slip transmission in NMLs have either used molecular dynamics (MD) simulations (Rao and Hazzledine 2000; Hoagland et al. 2002, 2004; Wang et al. 2008; Anderson et al. 1999; Wang and Misra 2011; Beyerlein et al. 2012), or atomistically informed micro-mechanical models (Akasheh et al. 2007; Zbib et al. 2011; Wang et al. 2014; Shao et al. 2018). Atomic scale simulations showed that beyond geometry alone, several critical factors affect slip transmission across the interface (e.g., dislocation core structure, emission probability of partials, changes in the stacking fault energy etc.). These studies suggest that transmission is easier across interfaces where the dislocation core remains intact and has a spread minimally at the interface. Several factors can affect the spread of the dislocation core at the interface in these laminate structures, including, crystallographic misorientation, misfit strains due to lattice mismatch between the different layers, interactions with misfit dislocations at the interface, and nonlinear elastic moduli at the interface. As is well known, MD simulations are restricted to small volumes and involve very high strain rates. On the other hand, continuum scale models in which larger volumes can be simulated under quasi-static loading scenarios, Ma et al. (2006); Mayeur and McDowell (2007); Van Beers et al. (2013); Chen et al. (2020), typically neglect the explicit treatment of interfaces and hence are unable to capture the fine processes dictating defect-interface interactions during the transmission process.

Dislocation dynamics can bridge information between the atomistic and larger length scale continuum models. Both the phase field dislocation dynamics (PFDD) where the discrete dislocations and the interfaces can be modeled explicitly (Bamney et al. 2021; Hunter et al. 2014; Hunter and Beyerlein 2014; Lei et al. 2013; Beyerlein and Hunter 2016; Zeng et al. 2016) as well as discrete dislocation dynamics (DDD) methods have been employed (Akasheh et al. 2007; Zbib et al. 2011; Zhou et al. 2010; Zhou and Lesar 2012; Li et al. 2009; El-Awady et al. 2016; Stricker et al. 2016; Burbery et al. 2017; Wei et al. 2019; Zhang et al. 2021). Akasheh et al. (2007) investigated the interaction of a single threading dislocation with interfacial dislocations and observed more accurate predictions of strength of the nano-layered structures with respect to corresponding experiments. Zbib et al. (2011) expanded on this work to include the appropriate stress fields for coherent and incoherent interfaces (as obtained from MD simulations), investigated the interaction with a single threading dislocation, and the resulting effect on the overall strength. In both these cases, the interface character was fixed and it was considered to be impenetrable, thus neglecting the dynamic evolution of the interface (such as dislocation glide within the interface or slip transmission) and its subsequent effect on the material response. Zhou et al. (2010); Zhou and Lesar (2012) investigated plasticity at nanoscales and size effect on the yield strength associated with small length scales for both single crystals and polycrystalline thin films, respectively. Even though their studies considered slip transmission, the geometry was restricted to single phases and idealistic conditions where no residual was formed at the interface. Li et al. (2009) considered a simplified 2D slip transmission model for investigating its effect in polycrystals with only two possible slip systems on either side of each grain and Papanikolaou et al. (2019) used 2D dislocation dynamics to study dislocation evolution in the interior of thin layers. Wang et al. (2014); Burbery et al. (2017); Shao et al. (2018) used atomistically

informed dislocation dynamics to incorporate a description of the interface and also the subsequent dislocation interactions at the interface. The interface-DDD model of Wang et al. (2014) considered several aspects of interface-dislocation interactions including dislocation nucleation, climb and glide of interface dislocations, and absorption of lattice dislocations in the interface. However, limited attention was given to the process of slip transmission across the interface, and the comprehensive effect of a network of dislocations on the dynamics of the system. Sobie et al. (2014) compared the mechanical responses for a bi-layer NML with a completely rigid and a completely shearable interface using DDD simulations. With their work, they demonstrated that the strength of the NML is not solely governed by the layer thicknesses, but also by the fate of the dislocations at the interface.

Even though DDD simulations have been used to investigate different phenomena related to dislocation interactions– such as dislocation mobility, grain size-effects, climb, and cross-slip– there has been limited effort in comprehensively capturing dislocation-interface effects, specifically for laminates with high elastic and plastic contrast between the constituent materials. Further, the aforementioned body of work has yet to consider the potential effects out of equilibrium state of interfaces. In recent work by Bamney et al. (2022), it was found that the resistance to slip transmission in interfaces (symmetric tilt grain boundaries in this case) that are far from a minimum energy equilibrium state (e.g., interfaces that have been impacted by dislocations) can be significantly lower from that of minimum energy equilibrated interfaces. Therefore, for ARB-processed NMLs, it is unclear how plasticity will proceed and evolve as the interface state (i.e. structure, geometry, energy) will likely depend on processing conditions and will evolve dynamically itself.

The present work aims to understand the role of dynamically evolving interfaces for ARB-processed NMLs. Specifically, focus is placed on quantifying the roles (i) of underlying crystallography (crystal orientation relationship) and (ii) the plastic anisotropy (difference in slip behavior) of the constituent materials of these NMLs on the mechanical response of NMLs. To this end, a previously developed DDD framework (Bertin et al. 2015; Bertin and Capolungo 2018; Capolungo and Taupin 2019; Bertin 2019) is extended and used to capture different dislocation/interface interactions and track the dynamic evolution of the interface under a high density dislocation network for NMLs. The model is then used to study dislocation-interface interactions on the relaxed dislocation microstructure and subsequent mechanical behavior of ARB processed NMLs, with body-centered cubic iron (bcc-Fe) and face-centered cubic copper (fcc-Cu) as the constituent materials. A general slip transmission module is integrated within DDD to allow dislocations to transmit across an interface and to accommodate any residual that is formed during the process. This new interface description also considers dislocation interactions between different phases at the interface– an effect insofar not studied in the context of DDD simulations.

This paper is structured as follows: "Computational framework" section briefly outlines the DDD framework and boundary conditions used in this study. Subsequently, the details of the slip transmission module and assumed rules for multi-phase dislocation interactions in this framework are described in "Modeling dislocation-interface interaction" section, followed by the details of the simulation geometry and boundary

conditions for the studied ARB processed Fe/Cu NML in "Simulation set-up" section. "Results" section shows the results from the DDD simulations highlighting the effect of layer thickness and interface type on the internal stresses and subsequent plastic response under interface normal compression and shear compression loading conditions. Finally, critical findings regarding the plasticity mechanism for each of the cases are discussed in "Discussion" section, and the corresponding conclusions of the work are summarized in "Conclusion" section.

## Computational framework

The multiscale DDD–FDM framework used for the dislocation dynamics simulation improves upon the generalized DDD code developed over the years by Bertin and Capolungo (2018); Capolungo and Taupin (2019); Kohnert and Capolungo (2021, 2022) and recently applied to investigate microstructure effects in metallic nanolaminates by Chakraborty et al. (2021). In this framework, the kinematics of the plastic flow from the sheared area of each discrete dislocation segment accounts for the compatible part of the continuum plastic distortion field. The incompatible part of the plastic distortion is computed by formulating an equivalent dislocation density tensor (i.e., the Nye tensor) field from the discrete dislocation network. The DDD equation of motion is based on Ghoniem et al. (2000) with a parallelized implementation described in Wang et al. (2006). Moreover, the code solves the micro-mechanical fields using a fast Fourier transform (FFT) algorithm that increases significantly the computational efficiency while preserving the accuracy of the fields at lower length scales. In what follows, we briefly describe the DDD–FDM within a FFT framework, and highlight its important equations. Subsequently, the details about the slip transmission module developed in this work is also provided, including the postulated laws governing dislocation interactions from different phases at the interface that are crucial in capturing the physics of deformation at lower length scales.

### Fast Fourier transforms to solve micromechanical fields

The total micro-mechanical strain is additively decomposed (small strain assumption) into elastic, $\epsilon^{el}$, and plastic, $\epsilon^{p}$, strains,

$$\epsilon_{ij} = \epsilon_{ij}^{el} + \epsilon_{ij}^{p} \tag{1}$$

Subsequently, solving Hooke's law,

$$\sigma_{kl} = \boldsymbol{C}_{klij}\left(\epsilon_{ij} - \epsilon_{ij}^{p}\right) \tag{2}$$

subject to the divergence free stress boundary condition $\left(\sigma_{kl,l} = 0\right)$ gives the solution for the micro-mechanical fields. $\sigma$ represents the Cauchy stress tensor, while $\boldsymbol{C}$ corresponds to the elastic stiffness of the constituent material(s). The total strain tensor is defined as the symmetric part of the displacement gradients $\left(u_{i,j}\right)$,

$$\epsilon_{ij} = \epsilon_{ji} = \frac{1}{2}\left(u_{i,j} + u_{j,i}\right) \tag{3}$$

The micro-mechanical strain ($\epsilon$) and stress ($\sigma$) fields are solved with a given description of the plastic strain ($\epsilon^p$), while the boundary value problem is solved using a Green's function method in Fourier space that provides an efficient way to solve such system of equations. These have been extensively used for meso-scale crystal plasticity simulations (Moulinec and Suquet 1998; Roters et al. 2010; Lebensohn et al. 2012).

#### Dislocation dynamics–field dislocation mechanics framework

The displacement gradient is additively decomposed into elastic, $\beta^e$, and plastic, $\beta^p$, distortions,

$$u_{i,j} = \beta^e_{ij} + \beta^p_{ij} \tag{4}$$

with the elastic and plastic distortions further decomposed into compatible ($\|$) and incompatible parts ($\perp$),

$$\beta^e_{ij} = \beta^{e,\|}_{ij} + \beta^{e,\perp}_{ij}, \tag{5}$$

$$\beta^p_{ij} = \beta^{p,\|}_{ij} + \beta^{p,\perp}_{ij} \tag{6}$$

Only the compatible distortions are curl free and can be represented as the gradient of a continuous field. Conversely, the incompatible elastic (or plastic) distortions are attributed to the presence of geometrically necessary dislocations, and its curl is given as,

$$-e_{jkl}\beta^p_{il,k} = e_{jkl}\beta^e_{il,k} = \alpha_{ij} \tag{7}$$

where $e$ is the permutation tensor and $\alpha$ represents the dislocation density (Nye) tensor with its components given by,

$$\alpha_{ij} = \frac{b_i t_j}{A} \tag{8}$$

for a given Burgers vector $\boldsymbol{b}$ and line direction $\boldsymbol{t}$. $A$ is the magnitude of the surface enclosed by the Burgers circuit. The incompatible distortions are solved using the Stokes-Helmholtz decomposition (Capolungo and Taupin 2019). It is important to note that this incompatible strain from the dislocation densities in the DDD scale is discrete, i.e. at each dislocation node, and is converted to a continuous meso-scale field for each FFT grid point using a regularization procedure to obtain a Nye tensor, $\alpha$, field in the meso-scale (Kohnert and Capolungo 2021). The compatible plastic distortion is then related to the shear caused due to dislocation glide,

$$\beta^{p,\|}_{ij} = \sum_s b^s_i n^s_j \gamma^s \tag{9}$$

on all the slip systems, $s$, with unit Burgers vector $\boldsymbol{b}^s$ and slip plane normal $\boldsymbol{n}^s$. The swept areas from the motion of each segment are summed over the simulation volume to construct the shear increment $\gamma^s$ for each system (Kohnert and Capolungo 2021). Together the symmetric part of both compatible and incompatible strain contributions constitutes

the macroscopic plastic strain. One thus obtains the respective full-field stress and strain fields.

### Modeling dislocation-interface interaction

To accurately predict the mechanical response of ARB processed NMLs, it is important to understand and model dislocation-interface interactions as these have profound implications for the microstructural state of the material following deformation. This work captures several attributes of such dislocation-interface interactions in the DDD–FDM framework by modeling different unit processes that could happen when dislocations reach a interface or phase boundary. Typically, dislocations at an interface or phase boundary can: Cho et al. (2020)

- absorb into the interface and become sessile,
- glide on the interface if its Burgers vector lies within the interface plane, or
- transmit into the adjacent grain or phase lying across the interface.

Slip transmission can, in principle, occur in cases where the Burgers vector magnitude and direction on both sides of the interface are exactly identical. Much more commonly, the Burgers vector must change in some way, and a residual dislocation is left on the interface to preserve continuity. When the Burgers vector of these residuals lies in the interface plane, the residual becomes glissile, and interfaces where this occurs are referred to as "shearable". All other residuals are sessile, with any motion requiring non-conservative (climb) processes. More generally, any non-zero misorientation angle $\theta$ between the incoming and transmission planes would require the propagation of multiple residuals within the interface to maintain continuity of the Burgers vector, and such cases will not be considered in this work.

The developments in this study capture each of the aforementioned events in a slip transmission framework integrated into the existing DDD–FDM approach discussed above. It models these mechanistic events in the presence of a network of dislocations, *and* tracks the dynamic evolution of dislocations at the interface. This capability is critical for studying ARB processed NMLs, as they have significantly higher dislocation density due to the severe plastic deformation processing condition (as compared to vapor deposited NMLs).

The slip system of transmitted dislocations follows the criteria of Lee et al. (1989) (LRB criteria), which:

- minimizes the misorientation between the traces of the incoming and outgoing slip planes at the interface,
- minimizes the magnitude of the residual Burgers vector formed at the interface, and
- maximizes the local resolved shear stress acting on the transmitted dislocation.

The first criterion is based on MD studies that suggest difficulty in slip transmission across an interface when there exists misorientation between the slip traces (Bachurin et al. 2010; Zhang et al. 2019). In this work we consider slip transmission only for events having zero misorientation, i.e., when the intersection line between the incoming and

outgoing slip planes lies within the interface plane. The second criterion minimizes the energy of the system upon a transmission event, as the energy of creating a residual dislocation scales with the square of the magnitude of the Burgers vector. Finally, transmission is allowed only if the resolved shear stress on the candidate transmitted slip system is greater than the critical resolved shear stress of that material, a modification to the LRB criteria suggested by Misra and Gibala (1999). These criteria have been demonstrated to provide good predictive capabilities for slip transmission across grain boundaries via in-situ transmission electron microscopy, and thus is chosen in this work over other slip transmission criteria reported in literature (Sangid et al. 2011). Figure 1 schematically shows the dislocation reactions upon a transmission event where the incoming segment (blue), $\boldsymbol{b_{inc}}$, on the interface dissociates into two dislocation segments: an outgoing system (red) segment, $\boldsymbol{b_{trans}}$, and another residual segment, $\boldsymbol{b_{res}}$, (white) on the interface with a magnitude defined as the difference between the incoming and outgoing Burgers vectors. Hence, modeling transmission events for a general case (where residuals are formed on the interface) using DDD involves positioning new nodes on the transmitted phase with the transmitted dislocation segments on the outgoing slip system, details of which are discussed next.

### Transmission kinematics

The underlying DDD–FDM method uses a node-based approach, where the nodal positions are updated based on the calculated nodal forces (Bertin and Capolungo 2018; Capolungo and Taupin 2019; Bamney et al. 2021; Kohnert and Capolungo 2022; Bamney et al. 2022). Herein, only the critical attributes of the newly developed transmission kinematics are discussed. For a detailed description of the DDD code and its capabilities refer to Bertin et al. (2015); Bertin and Capolungo (2018); Bertin (2019); Kohnert and Capolungo (2021). The dislocation nodes are fully described by their position, velocity, nodal force, host phase, and the segments which connect them to neighbor nodes. This information is required to perform dynamic evolution of the nodal positions, dislocation-dislocation interactions, and dislocation segment re-meshing. These operations collectively evolve the dislocation network attributes (such as dislocation density, junction

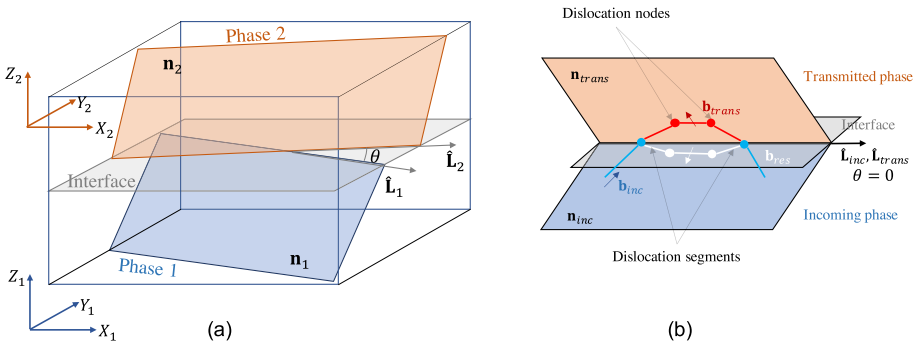


**Fig. 1** **a** shows the geometric aspect of the laminate structure with a misorientation angle $\theta$ between the incoming, $\hat{\mathbf{L}}_1$, and outgoing, $\hat{\mathbf{L}}_2$, slip traces. This work considers transmission cases for $\theta = 0$, as shown schematically in (**b**) along with a slip transmission event where the incoming dislocation with Burgers vector $b_{inc}$, transmits from the incoming slip plane, $n_{inc}$, in phase 1 onto the transmitted slip plane, $n_{trans}$, in phase 2 with a Burgers vector $b_{trans}$. In this process, a residual Burgers vector of $b_{res} = b_{inc} - b_{trans}$ is formed at the interface (white)

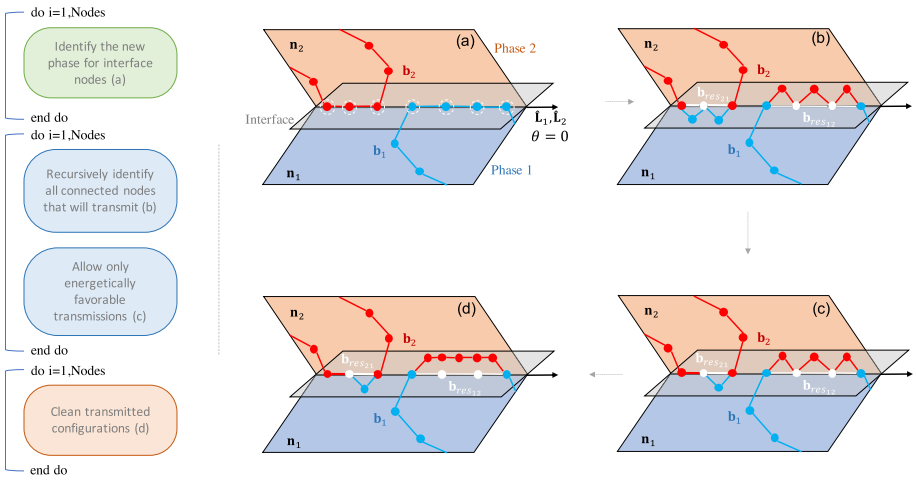


**Fig. 2** Schematic representation of the slip transmission module developed in this work, with the critical algorithmic operations shown in the left block chart. The corresponding sketches for these operations are shown sequentially on the right for two exemplary dislocations approaching (and transmitting across) the interface from both phases. Each plausible transmission event for a dislocation segment results in creation of a new dislocation node and two new dislocation segments, as shown here

density, and their types) over time. Thus, to modeling a transmission event involves creating new dislocation segments and nodes and updating the nodal attributes accordingly.

Figure 2 highlights the main blocks and algorithmic structure of the transmission framework proposed here. First, nodes are not allowed to migrate across interfaces due to glide alone. If a node would cross an interface during glide it is halted at the interface. The interface plane is then added to the glide planes associated with the node, such that it can glide only along the trace of its glide plane on the interface plane. Possible transmission events are evaluated at each time step after all glide motion is resolved.

Transmission is considered for nodes associated with an interface. First, the host and transmission phases[1] are identified. Transmission is evaluated on a segment-by-segment basis. Segments become transmission candidates if (a) both nodes bounding the segment lie on the same interface, (b) the forces acting on these nodes point away from their host (origin) phase and (c) the segment does not glide in the interface plane. For each candidate segment, the modified LRB criteria (discussed previously) are applied to determine the outgoing slip system and whether to execute a transmission event.

If all criteria for transmission are met, a new node is placed on the corresponding slip system in the new phase. The segment remaining in the interface becomes a residual, and it's Burgers vector is modified accordingly (the segment is removed if the residual Burgers vector happens to be zero). Two new segments are created, connecting the new transmission node to each existing interface node. Using the same transmitted slip system, the same criteria are immediately applied any neighboring segments. Transmission proceeds recursively along the dislocation line until the segment are no longer viable transmission candidates or the LRB criteria are no longer met. The recursion approach

[1] For the purpose of the manuscript and the DDD–FDM code, a phase is defined as a region of the solid with a uniform crystal lattice (i.e., a different material, a different grain, a precipitate, etc. are all unique phases) and different phases are separated by an interface.

minimizes the chances of nearby segments transmitting onto alternating slip planes with similar resolved shear stress.

When multiple connected segments are transmitted in the same step, nodes shared by the transmitted segments must be dissociated from the interface. For each such shared node, a new node is created in the transmitted phase, bisecting the positions of the adjacent transmitted nodes. Transmitted segments are connected to these dissociated nodes, instead of the nodes remaining on the interface. The interface nodes now only connect to the residual segments (if any) as shown schematically in (c)-(d) in Fig. 2. Transmitted configurations are checked for positive dissipation by recalculating the force on transmitted nodes for the updated configuration. The event is allowed only if the projected force along the transmitted slip direction remains positive. This allows for the incorporation of the effect of local microstructure (neighboring dislocation network with short and long-range interactions) along with the applied loading condition on the success of a transmission event. Where local forces do not allow segments to transmit, these segments are restored to the interface with and can be subsequently reconsidered for transmission in the next timestep.

The aforementioned algorithm allows one to model transmission of dislocation segments across any general interface. However, another critical aspect that governs the kinematic response and evolution of dislocation segments, especially at the interface, are the local interactions that can happen between different dislocations at the interface. Since, this work concerns with NMLs with different materials, the dislocation interactions at the interface can also involve dislocations coming from different phases, which is addressed subsequently.

#### Local interactions of interface dislocations

Interfaces may contain several different kinds of dislocations, including bulk dislocations from both adjacent phases (materials) as well as the residual dislocations that may be created on the interface following a transmission event. Based on the simulation geometry and the Burgers vector of the interface dislocations, the dislocations may be sessile or glissile on the interface. These dislocations can interact with one another, which may govern the overall response of the material. In DDD, dislocation-dislocation interactions are governed based on certain rules, which have been well established through analytical solutions of junction formation (Dupuy and Fivel 2002; Weygand et al. 2002; Kubin 2013; El-Awady et al. 2016), for dislocations in the same phase/material. However, dislocation interactions between different material systems at the interface, such as between fcc-bcc NMLs studied in this work, are seldom addressed in the literature. We propose interaction rules for dislocations at interfaces originating from different phases (e.g. fcc and bcc). There are three categories of potential interactions between a pair of interface dislocations: both sessile, both glissile, and one of each.

We do not allow interactions between two sessile interface dislocations, as neither can glide. The second category is also relatively straight forward. Two glissile dislocations can interact to either annihilate each other (equal and opposite Burgers vector) or create a junction that can also glide on the interface plane. For the interaction between a glissile and a sessile dislocation, the resulting junction must be sessile, and is given the properties of the sessile dislocation (i.e., phase and line direction). However, sessile junctions

on the interface are still valid transmission candidates, and can act as sources for transmission if they satisfy the previously mentioned transmission criteria.

### Simulation set-up

A critical aspect of any DDD simulation is the generation of the initial microstructure. Oftentimes, DDD simulations are started with random seeds of Frank–Read sources in the simulation volume, which are then relaxed to obtain the initial microstructure, thereby ignoring the effect of any processing history on the initial microstructure. Such a strategy is not suitable for simulating the mechanical behavior of ARB processed NMLs that are associated with severe plastic deformation conditions that would significantly govern the initial dislocation microstructure in these systems (Chakraborty et al. 2021). To preferentially populate the slip systems activated during formation the ARB-processed fcc-Cu and bcc-Fe NMLs studied in this work, the initial microstructure is generated using a fixed load compression boundary condition on pre-seeded glide loops described below.

A random seed of dislocation loops are placed in both the Cu (slip system: $\{1\,1\,1\}\langle 1\,1\,0\rangle$) and the Fe (slip systems: $\{1\,1\,0\}\langle 1\,1\,1\rangle$ and $\{1\,1\,2\}\langle 1\,1\,1\rangle$) layers. On average, 3 dislocation loops per slip system were placed with their centers selected a random within the host layer, and with a loop size of similar magnitude to the layer thickness. During loading, a very high state of fixed stress well above the yield point is imposed for a relatively short amount of time (2000 timesteps) with components

$$\boldsymbol{\sigma} = \begin{bmatrix} -0.6 & -0.004 & 0.002 \\ -0.004 & -0.2 & 0.08 \\ 0.002 & 0.08 & -1.5 \end{bmatrix} \text{GPa} \tag{10}$$

orientated consistent with the rolling process. Such a state of stress corresponds to a strain state with $\varepsilon_{ZZ} = -0.02, \varepsilon_{YY} = 0.01, \varepsilon_{YZ} = 0.002$[2], for pure Cu with the remaining strain components being zero. With this boundary condition the sample directions, X, Y, Z, correspond to the transverse direction (TD), rolling direction (RD) and normal direction (ND), respectively. During loading, the von Mises stress is $\approx 1.2$ GPa, with corresponding von Mises strain of 2.01 %.

The compression loading stage promotes rapid dislocation multiplication on the systems expected to be activated during ARB. After 2000 steps, the load is removed for a significantly longer relaxation period (60000 steps) under zero stress applied to the representative volume element (RVE). In both cases, the time discretization is $1 \times 10^{-13}$ seconds. The configuration is considered to be relaxed when the average bulk dislocation density evolution saturates. An example of this process is shown in Fig. 3 with a layer thickness of 200 nm. The total volume $\left(64 \times 10^6\ \text{nm}^3\right)$ is discretized using $64 \times 64 \times 64$ voxels for the FFT calculations. Thus while the pre-compression creates continuous networks, favoring slip systems activated by the ARB process, the total strain reached within DDD remains significantly lower than those achieved in the real process.

[2] Note that relatively small values for the shear stress components $\sigma_{XY}$ and $\sigma_{XZ}$ instead of zero are imposed to activate certain slip systems in the material.

First, we compare the microstructural attributes and the residual stresses in the relaxed configuration for a fcc-Cu/bcc-Fe NML with a {1 1 2}/{1 1 2} type Kurdjomav-Sachs (KS) interface (of type II (Wang et al. 2014)). The shear moduli of Cu and Fe are 47.34 and 82.35 GPa respectively, and Poisson's ratios of 0.323 for Fe and 0.281 for Cu are used. The interface configuration is such that the (1 1 2) plane of fcc Cu coincides with the (1 1 2) plane of bcc Fe and is the interface plane, i.e. sample Z axis. The corresponding (1 $\bar{1}$ 0) in the Cu phase is aligned with the (1 1 $\bar{1}$) plane of the Fe layer, both noraml to then Y axis. Moreover, the simulation volume is rotated by 20° ($\phi$ in Fig. 3) about sample Z axis to avoid self-annihilation of the dislocation loops due to the periodic boundary conditions. The Peierl's barrier for Cu, 5MPa, is selected to be much smaller than that in the Fe layers 100MPa, with corresponding drag coefficients being $1.5 \times 10^{-5}$ and $1.5 \times 10^{-4}$ Pa s (Kubin 2013; Sills et al. 2016). Since the interface dislocation properties are not well-established, this work assumes the dislocations at the interface to have the properties of the softer fcc Cu layer. For the present work, the dislocation properties (i.e., mobility and friction stresses) are kept same for edge and screw dislocations for both the systems for simplicity. Moreover, based on the energy of the configuration, transmission only occurs from the stiffer Fe phase to the softer Cu phase, as explained later in Appendix A.

An ideal final dislocation microstructure for the present study would be such that it contains dislocations on multiple slip systems in both layers, shown via the histogram of the slip system distributions in Fig. 3, thus avoiding single slip (or similar biased) deformation responses. The relaxed configurations are then subjected to loading conditions of compression along the sample Z direction, (ND), as well as a shear compression in the sample YZ plane to understand the mechanical behavior and plastic mechanisms through the DDD simulations. Multiple relaxed configurations are generated for each geometry, starting with different initial random seeds for the dislocation loops in order to have a more representative understanding. Subsequently, the effect of different

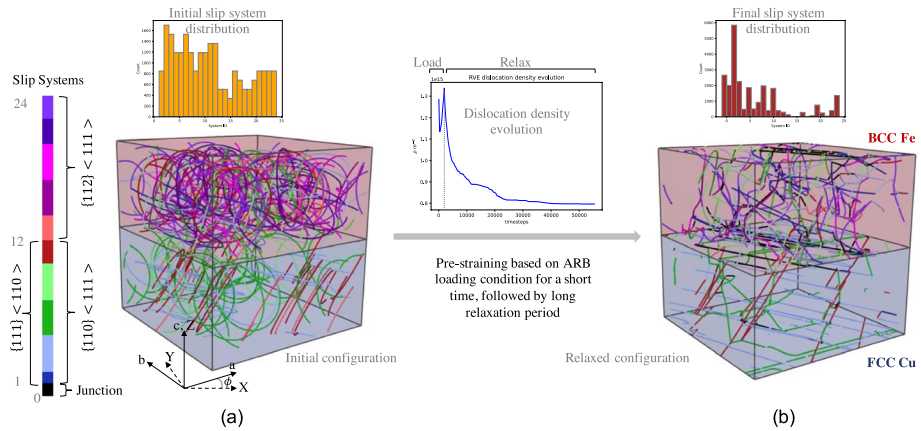


**Fig. 3** Overall simulation strategy starting with a random seed of initial dislocation loops (**a**) for both layers. Each color of the loop represents different slip systems in the fcc (Cu) and bcc (Fe) layers with a layer thickness of 200 nm. The relaxed network configuration after the pre-strain-relaxation loading condition is also shown (**b**), which is used to perform the subsequent loading simulations of the sample Z normal compression and sample YZ shear compression. The pre-strain-relaxation condition involves a load stage where a high stress state is imposed for a short amount of time, followed by a long relaxation period under zero stress boundary condition. This loading stress state is selected to emulate (at least partially) the ARB processing condition with sample Y and Z being the normal direction (ND) and rolling directions, respectively

material systems is also investigated by performing the aforementioned investigation for a {1 1 1}/{1 1 0} KS interface (of type I (Wang et al. 2014)) for the fcc-Cu/bcc-Fe layers with a fixed layer thickness of 200 nm.

## Results

The developed framework is used to investigate the effect of layer thickness and interface type for ARB processed Fe/Cu NMLs. As mentioned, the effect of the ARB processing condition is incorporated with the pre-strain relaxation boundary condition to generate the initial dislocation network microstructure. Such conditions will introduce residual stresses in these dislocation network microstructures, thus affecting their subsequent mechanical behavior.

This section studies the mechanical response of NMLs for two different cases of Fe/Cu NMLs–(i) having the same interface type, of {1 1 2}/{1 1 2}, but with different layer thicknesses; and (ii) having same layer thickness of 200 nm but with different interface type (crystal orientation) between the fcc and bcc layers. The ND, RD, and TD coincide with sample Z, Y, and X axes, respectively. Subsequently, for each of the cases we also investigate their mechanical behavior by performing strain rate controlled compression simulations along the sample Z (ND) direction, as well as a shear compression in the sample YZ plane (corresponding to the ND-RD plane in our convention).

### Effect of layer thickness

Figure 4 plots the residual stress in the Cu (blue markers) and Fe (red markers) layers in the three different directions of TD (left column), RD (middle column), and ND (right column) for both 200 nm (top row) and 400 nm (bottom row) layer thicknesses. The residual stress is calculated by summing up the stress tensors for all the FFT voxels in the particular layer and taking a numerical average. Each marker corresponds to a different initial random seed of starting dislocation loops, i.e., different equivalent microstructures. The simulations predict a generally larger residual stress for smaller layer thicknesses, however, there is a slight variability in these stress component values among each equivalent microstructure, except those in the TD ((a) and (d) in Fig. 4) where the values are almost zero. Moreover, for the 200 nm layer thickness, the average residual stress component in *both* the RD and ND ((b) and (c) in Fig. 4) is generally tensile in the Fe layer (red) and compressive in the the Cu layer (blue). Conversely, one sees a change in sign for the 400 nm thick NML, where the Fe layer is generally tensile along RD and compressive along ND ((e) and (f) in Fig. 4). This indicates the variability in initial configuration of these networks depending on the initial seed of dislocation loops, and hence is a critical aspect of understanding these systems through DDD simulations. Figure 5 plots the dislocation density evolution in the bulk and interface during this pre-strain-relaxation step of generating the dislocation network configurations. As expected, a higher average bulk dislocation density (magenta) of $\approx 1 \times 10^{15} m^{-2}$ for the 200 nm (solid curves) thick material is observed, as compared to the 400 nm thick NML (dashed curves) with a density of $\approx 1 \times 10^{14} m^{-2}$, Fig. 5a. For both cases the Fe layer is predicted to have a higher dislocation density than the Cu layer, (b) in Fig. 5. A higher interface dislocation density is predicted for thinner layers during the microstructure generation.

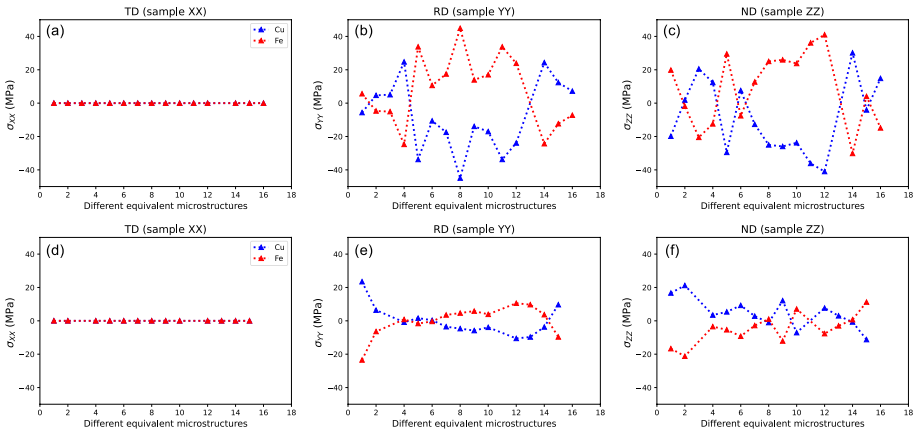


**Fig. 4** Average residual stresses in the fcc (blue markers) and bcc (red markers) for a {1 1 2}/{1 1 2} Fe/Cu NML with a layer thickness of 200 nm, (**a**-**c**), and 400 nm, (**d**-**f**). Left, center, and right columns show the components along the transverse direction (TD; sample XX), rolling direction (RD; sample YY), and normal direction (ND; sample ZZ), respectively, for each layer thickness, based on the convention used in the manuscript. The corresponding Euler angles (in radians) are $\phi_1 = 0.34906585, \Phi = 0.61547971, \phi_2 = 0.78539816$ for the Cu phase, and $\phi_1 = 5.06145483, \Phi = 0.61547971, \phi_2 = 0.78539816$ for the Fe phase

However, the areal dislocation density (i.e. line length per unit volume) may not make for meaningful comparisons as the layer thickness changes. For this reason, the linear density (line length per unit area, $\rho L$) is also shown. On this measure, the densities are more similar, but still significantly higher for the composite with thinner layers. Note that this trend is consistent with experimental characterization of interface dislocation content in rolled Fe/Cu composites (Pohl et al. 2023).

Through these simulations, the number of possible slip transmission events are also compared for the different layer thicknesses during the microstructure generation step, and shown in Fig. 5d. A higher number of possible transmission events can, indeed, be considered to be a reflection of a higher slip transmission probability[3]. Again, the difference in interface area and simulation volume may complicate a direct comparison, so the number of transmission events is divided by the total line length on the interface. This generates a transmission probability per unit length, shown as grey curves for each case. Both measures reflect a substantial increase in transmission frequency for thinner layers. The simulations, thus, predict both higher slip transmissibility and dislocation density as layer thickness decreases.

Subsequently, the mechanical behavior of these NMLs as a function of layer thickness is also compared by loading in two different directions– normal direction compression along sample Z (ND) Fig. 6; and a shear compression along the sample YZ plane Fig. 7, with a strain rate of $-1 \times 10^5 s^{-1}$. The average macroscopic response is predicted to be significantly different in ND loading as compared to shear loading, as evident from the distinctively different stress-strain plots ((c) in Figs. 6 and 7) for both layer thicknesses. Furthermore, the material appears much softer ($\approx 3$ times) under shear as compared to normal direction loading. The respective dislocation density evolution are also shown

[3] It is important to note that not all the segments that are identified to transmit will actually transmit to the bulk of the transmitted phase, such will be governed by the local driving forces.

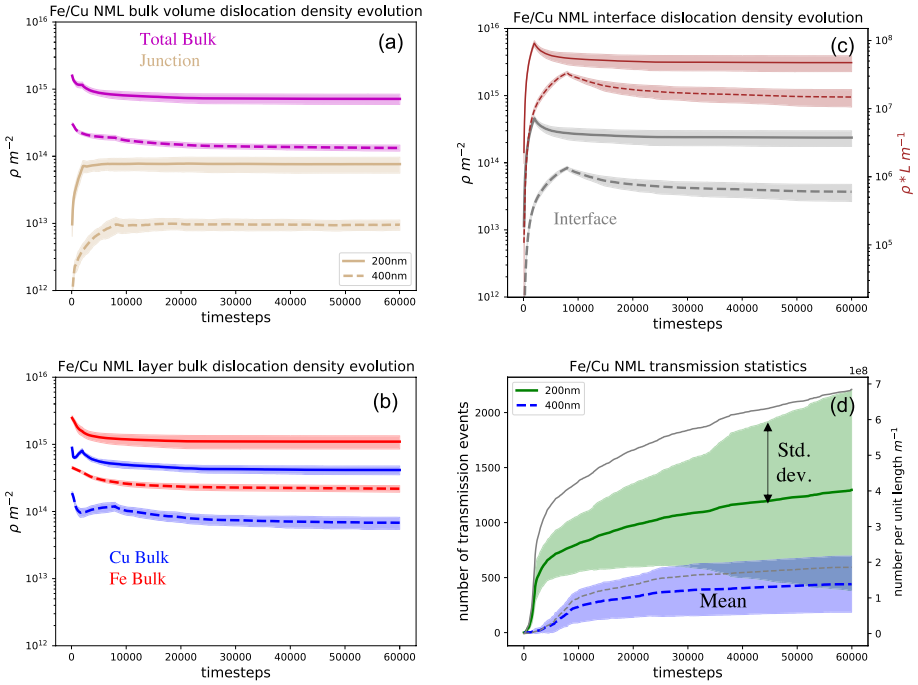


**Fig. 5** **a** plots the total volume averaged bulk (magenta) and junction density (tan) evolution during the pre-strain-relaxation step of microstructure generation for both 200 nm (solid curves) and 400 nm (dashed curves) layer thicknesses for a {1 1 2}/{1 1 2} Fe/Cu NML. Similarly, (**b**) plots the corresponding bulk dislocation density evolution for the Fe (red) and Cu (blue) layers, and (**c**) plots the interface dislocation density evolution in both areal (gray) and linear (red) units. Finally, the transmission propensity as a function of plausible transmission events from the Fe to the Cu phase is also plotted in (**d**) during the microstructure generation step. In each of the figures, the solid lines correspond to the mean result from ≈ 15 simulations, with the filled area highlighting the standard deviation between the runs for all the plots. Also, the gray lines in (**d**) correspond to the (mean) number of these transmission events normalized by the average interface density for both 200 nm (solid) and 400 nm (dashed) undermine their role on the respective transmission propensity

for the two cases, (a), (b) in Figs. 6 and 7. Interestingly, the directional dependence in the mechanical behavior is also reflected in the dislocation density evolution, where for ND compression the interface dislocation density and the Cu dislocation density increases with load, while the Fe dislocation density decreases, especially for the 200 nm layer thickness. This indicates more bcc dislocations are reaching the interface and are able to transmit to the fcc phase during the ND compression loading. Qualitatively, there seems to be less differences for the simulated responses between the different layer thicknesses, as compared to shear compression, which shows much steeper hardening for the larger layer thickness, Fig. 7c. Also, the transmission propensity during loading seems to be generally higher for the larger layer thickness, which is expected as a lower activation stress is needed for larger layer thicknesses, (d) in Figs. 6 and 7. Again, it is important to note that the transmission propensity does not correspond to actual successful transmitted dislocations that go into the bulk of the transmitted phase, but rather provides a more qualitative estimation of the transmission events.

### Effect of interface type

The effect of the orientation relationship of the constituent materials for ARB processed NMLs is also studied through DDD simulations, by repeating the previous

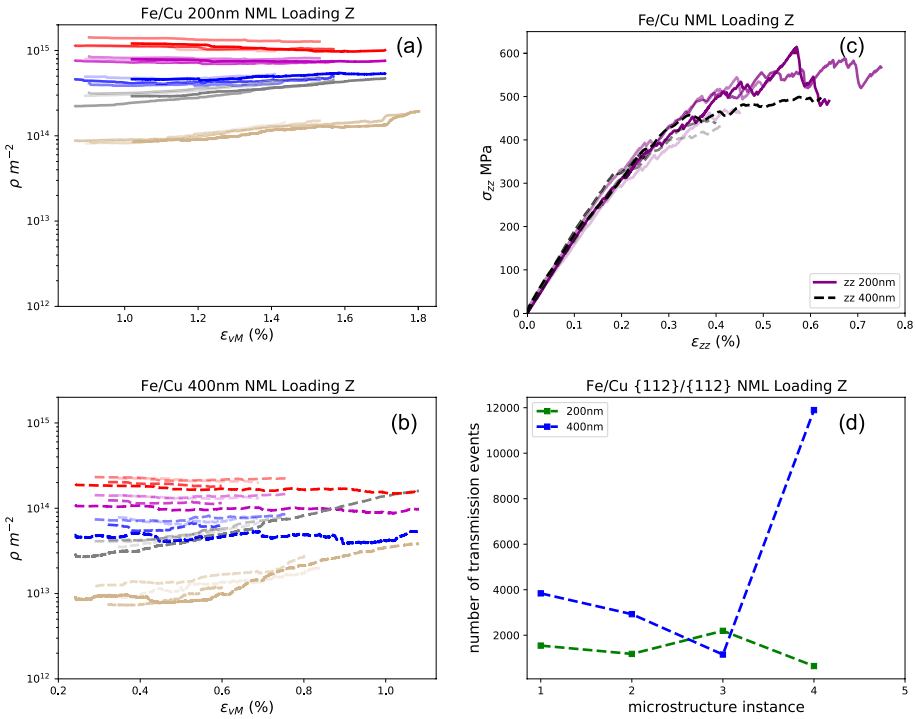


**Fig. 6** **a** and **b** plot the dislocation density evolution as a function of volume averaged von Mises strain for the total bulk (magenta), junctions (tan), Fe bulk (red), Cu bulk (blue), and interface (gray) for 200 nm (solid) and 400 nm (dashed) thick {1 1 2}/{1 1 2} Fe/Cu NML, respectively, during sample Z compression loading. The corresponding directional stress-strain response is plotted in (**c**), for both 200 nm (purple) and 400 nm (gray) layer thicknesses. Each loading simulation is repeated with 4 random initial relaxed configurations as represented by the different curves for each case. The total number of possible transmission events for the 4 loading simulations for each layer thickness is also shown in (**d**). For all the dislocation density plots for the Cu and Fe layers (**a** and **b**), different shades of each color correspond to the 4 different configurations

analysis of microstructure generation and compression loading for a {1 1 0}/{1 1 1} KS-type Fe/Cu NML with a 200 nm layer thickness. Figure 8 compares the residual stresses in the different directions (TD, RD, and ND) for a {1 1 2}/{1 1 2}, (a)-(c), and a {1 1 0}/{1 1 1}, (d)-(f), Fe/Cu NML with 200 nm layer thickness, as obtained from ∼15 equivalent DDD simulations starting with a different random seed for the initial dislocation loops. The values of the residual stresses for both types of NMLs are similar in magnitude, however, for the {1 1 0}/{1 1 1} interface the Cu layer seems to be generally under a compressive state of stress while the Fe layer is under a tensile state of stress–opposite to that generally observed for the {1 1 2}/{1 1 2} interface. The dislocation density evolution during the microstructure generation is also qualitatively similar for the two types of interfaces, Fig. 9a-c, however the slip transmission propensity for the {1 1 0}/{1 1 1} interface is much lower than the {1 1 2}/{1 1 2} interface. Also, it is interesting to note that the respective bulk densities are higher for the {1 1 2}/{1 1 2} interface (solid curves), while the interface density is nominally higher for the {1 1 0}/{1 1 1} interface (dashed curves). Thus, the interface type also affects the internal stresses, and the transmissibility for these ARB processed NMLs.

Next, the mechanical behavior of the {1 1 0}/{1 1 1} Fe/Cu interface is studied by compressing along the interface normal direction and shear compression on the sample YZ plane, as in the previous section. Figure 10c compares the

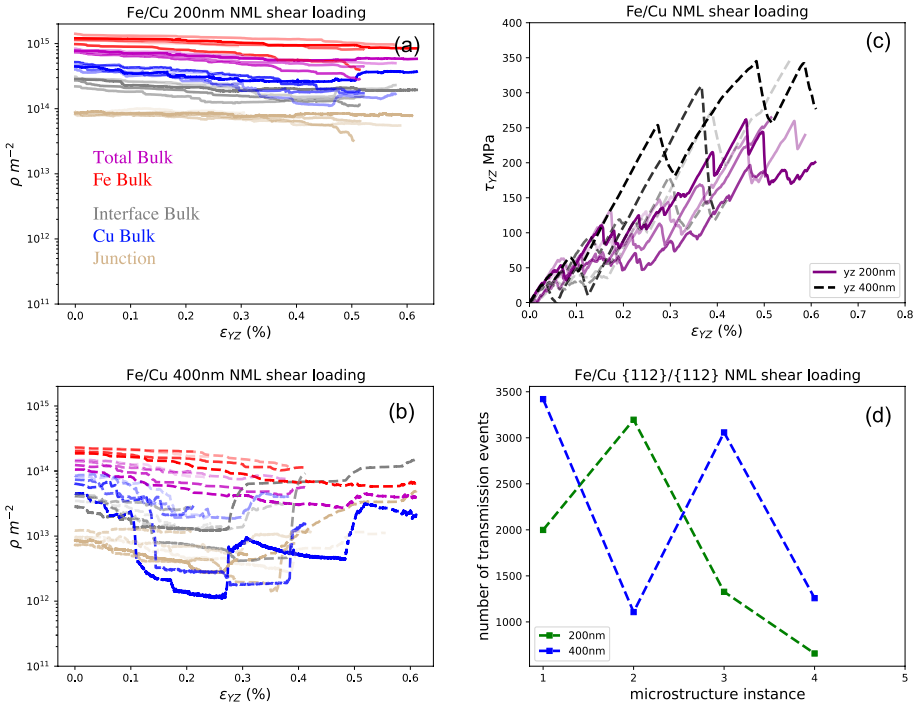


**Fig. 7** **a** and **b** plots the dislocation density evolution as a function of volume averaged von Mises strain for the total bulk (magenta), junctions (tan), Fe bulk (red), Cu bulk (blue), and interface (gray) for 200 nm (solid) and 400 nm (dashed) thick {1 1 2}/{1 1 2} Fe/Cu NML, respectively, during shear YZ compression loading. The corresponding shear stress-strain response is plotted in (**c**), for both 200 nm (purple) and 400 nm (gray) layer thicknesses. Each loading simulation is repeated with 4 random initial relaxed configurations as represented by the different curves for each case. The total number of possible transmission events for the 4 loading simulations for each layer thickness is also shown in (**d**)

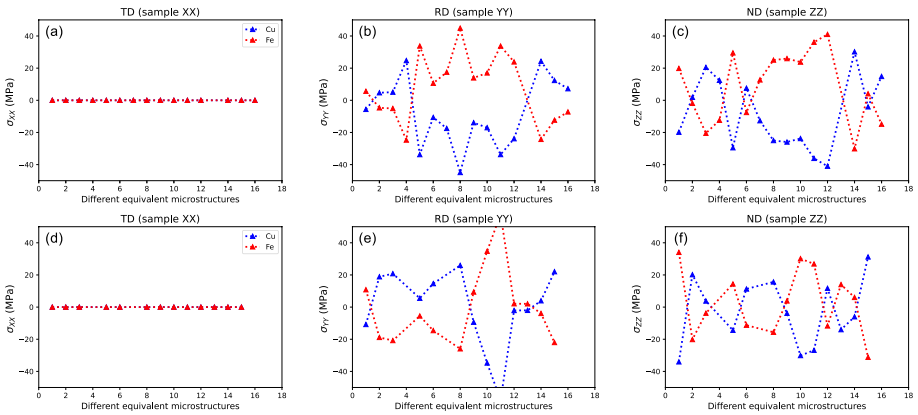


**Fig. 8** Average residual stresses in the fcc (blue markers) and bcc (red markers) for an ~200 nm thick {1 1 2}/{1 1 2}, (**a**-**c**), and a {1 1 0}/{1 1 1}, (**d**-**f**), Fe/Cu NML. Left, center, and right columns show the components along the transverse direction (TD; sample XX), rolling direction (RD; sample YY), and normal direction (ND; sample ZZ), respectively, for each layer thickness, based on the convention used in the manuscript. The corresponding Euler angles (in radians) are $\phi_1 = 0.34906585$, $\Phi = 0.95531662$, $\phi_2 = 0.78539816$ for the Cu phase, and $\phi_1 = 2.8751788$, $\Phi = 1.57079633$, $\phi_2 = 0.78539816$ for the Fe phase

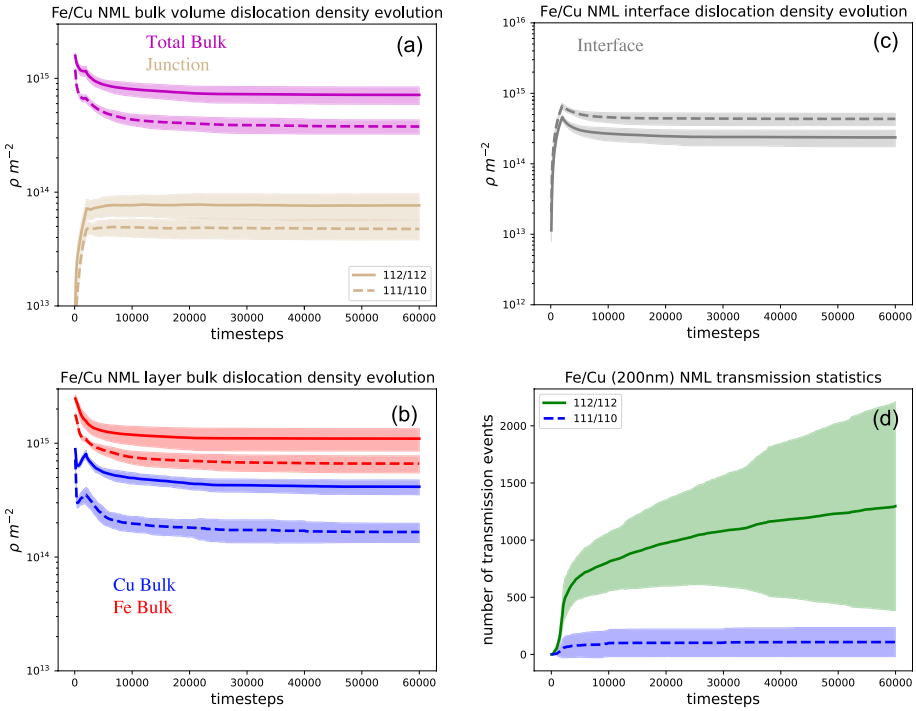


**Fig. 9** The dislocation density evolution plots of, (**a**), the total volume averaged bulk (magenta) and junction density (tan) during the pre-strain-relaxation step of microstructure generation for a {1 1 2}/{1 1 2} (solid curves) and a {1 1 0}/{1 1 1} (dashed curves) Fe/Cu NML with 200 nm layer thickness. Like before, (**b**) plots the corresponding bulk dislocation density evolution for the Fe (red) and Cu (blue) layers, with (**c**) plotting the respective interface dislocation density evolution (gray) for the two NMLs. The transmission propensity as a function of plausible transmission events from the Fe to the Cu phase is also plotted in (**d**) during the microstructure generation step

corresponding mechanical behavior of a 200 nm thick Fe/Cu NML under ND (sample Z) compression loading between a {1 1 2}/{1 1 2} interface (purple solid curves) and a {1 1 0}/{1 1 1} interface (dashed gray curves). The mechanical response is slightly "harder" for the {1 1 0}/{1 1 1} interface, as compared to the {1 1 2}/{1 1 2} interface NML. Additionally, a similar dislocation density evolution during loading is predicted for the two interface types, (a) and (b) in Fig. 10. Moreover, the transmission propensity (Fig. 10d) of the {1 1 0}/{1 1 1} interface (blue) also appears to be much lower than the {1 1 2}/{1 1 2} interface (green). This is consistent with the observation during microstructure generation (Fig. 9d) and can be attributed to higher possibility of dislocations gliding on the interface instead of transmitting, as the interface plane is a glide plane for *both* Fe and Cu phases for the KS-type I interface NMLs. The model predicts similar response when loaded in shear compression in the sample YZ plane, Fig. 11, with similar dislocation density evolution between the two types of interfaces, and a lower transmission probability for the {1 1 0}/{1 1 1} interface.

## Discussion

The initial microstructures generated with the pre-strain-relaxation boundary condition, using the proposed DDD–FDM framework incorporating slip transmission and multi-phase dislocation interactions suggests the presence of residual stresses in

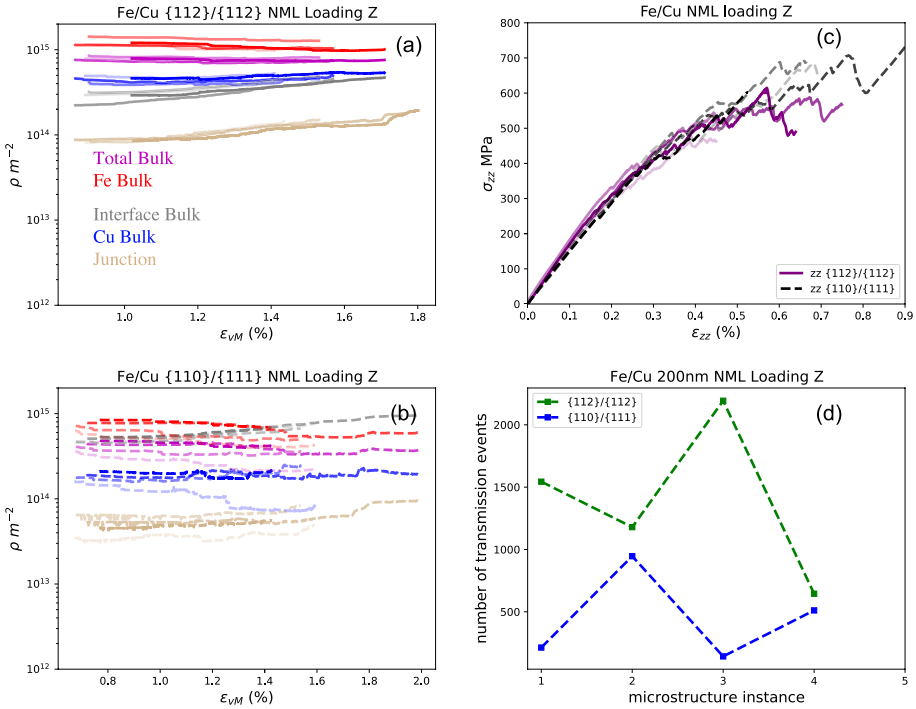


**Fig. 10** Comparing mechanical behavior under interface ND compression loading of 200 nm thick Fe/Cu NMLs with {1 1 2}/{1 1 2} and {1 1 0}/{1 1 1} interfaces. **a** and **b** plots the total bulk (magenta), junction (tan), Fe bulk (red), Cu bulk (blue), and the interface (gray) dislocation density evolution during the ND compression loading for the {1 1 2}/{1 1 2} (solid curves), and {1 1 0}/{1 1 1} (dashed curves) interfaces, respectively. As before, (**c**) plots the corresponding directional stress-strain response for {1 1 2}/{1 1 2} (purple solid curves), and {1 1 0}/{1 1 1} (gray dashed curves) under the ND compression loading. Similarly, transmission propensity as a function total transmission events is also compared for the two interfaces, (**d**), with the {1 1 2}/{1 1 2} interface (green) showing a higher propensity as compared to the {1 1 0}/{1 1 1} (blue) interface

the relaxed configuration, that tend to be higher for smaller layer thicknesses, Fig. 4. Changing the interface type from a {1 1 2}/{1 1 2} to a {1 1 0}/{1 1 1} does, indeed, affect the sign of the residual stress components in the Fe and the Cu layers, but not so much their magnitudes, Fig. 8.

In this work, we assume the transmission propensity to be represented by the number of bcc-Fe dislocation segments on the interface that can transmit to the fcc-Cu phase. As mentioned previously, this is an approximation, since not all the segments identified as potentially transmissible can successfully glide into the bulk of the transmitted phase, which depends on the local driving forces. With this assumption, the model predicts highest transmission propensity for a 200 nm thick Fe/Cu NML with a {1 1 2}/{1 1 2} interface, among the different cases studied here. This propensity decreases for a {1 1 0}/{1 1 1} interface, which aligns with findings from atomistic simulations (Wang et al. 2012, 2014). Moreover, a larger layer thickness also results in lower transmission propensity during this pre-strain-relaxation process of microstructure generation. The former can be attributed to the higher plausibility of interface dislocations to glide on the interface plane (since a {1 1 0}/{1 1 1} interface is a glide plane for both Fe and Cu phases) which competes with slip transmission, while,

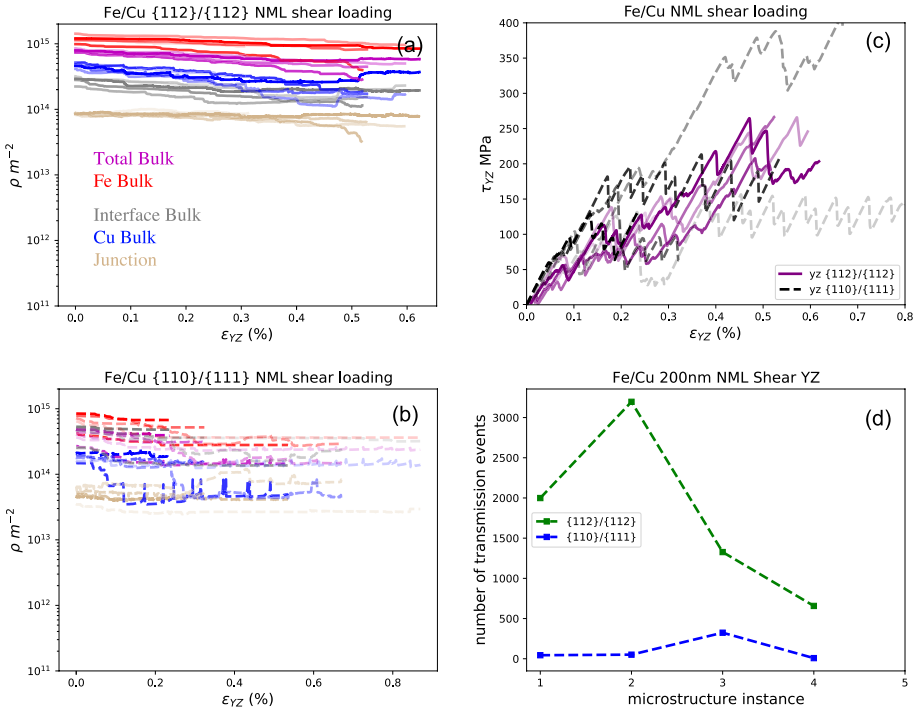


**Fig. 11** Comparing mechanical behavior under shear YZ compression loading of 200 nm thick Fe/Cu NMLs with {1 1 2}/{1 1 2} and {1 1 0}/{1 1 1} interfaces. **a** and **b** plots the total bulk (magenta), junction (tan), Fe bulk (red), Cu bulk (blue), and the interface (gray) dislocation density evolution during the shear compression loading for the {1 1 2}/{1 1 2} (solid curves), and {1 1 0}/{1 1 1} (dashed curves) interfaces, respectively. As before, (**c**) plots the corresponding shear stress-strain response for {1 1 2}/{1 1 2} (purple solid curves), and {1 1 0}/{1 1 1} (gray dashed curves) under the ND compression loading. Similarly, transmission propensity as a function total transmission events is also compared for the two interfaces, (**d**), with the {1 1 2}/{1 1 2} interface (green) showing a higher propensity as compared to the {1 1 0}/{1 1 1} (blue) interface

the later can be due to the lower interface dislocation density for larger layer thicknesses[4], (c) in Fig. 5, as well as lower internal stresses.

It should be noted that the short range correction terms used in this methodology are only precise in a uniform elastic medium. This implies that the forces acting on dislocations within one FFT voxel of the interfaces - while of the correct magnitude - have lower accuracy than those acting on dislocations in the bulk. This can influence the applied stress at which a particular segment will be identified as attempting to nucleate a transmission event but will not determine whether a transmitted dislocation can fully propagate into bulk material. Further, the line tension of interface dislocations will be similarly impacted, but assessing this more accurately requires a more detailed understanding of the core structure and energetics of defects on the interface.

In the relaxed configuration the softer Cu layer always has a lower dislocation density when compared to the stiffer Fe layer, indicating an influence of the pre-strain-relaxation processing condition on the initial relaxed configuration that agrees with previous work (Chakraborty et al. 2021). A higher dislocation density in the bcc-Fe layers is

[4] Lower interface dislocation density indicates a fewer number of dislocation segments at the interface, and hence, a lower overall transmission propensity of the material.

due to a high Peierls barrier of dislocations in this phase (as compared to fcc-Cu phase), thus requiring a higher driving force for their motion. Slower dislocation motion leads to annihilation of fewer dislocation segments, and hence, a higher overall dislocation density. Furthermore, a larger number of available slip systems in the Fe layer (24 as compared to 12 for fcc-Cu) can lead to higher sessile dislocation junctions, thereby, further restricting their motion in this phase.

In addition, the above analysis with multiple initial random seeds for the dislocation loops highlights the variability that is associated with the initial microstructure generated using DDD simulations, both in their residual stresses and their transmission propensity – attributed to the variability in active slip systems and their dynamic interactions in each layer. Hence, such structures should be considered more as a statistical volume elements representing specific configurations in the overall microstructure of the actual bulk material, rather than a representative volume element which is the norm for meso-scale (e.g. crystal plasticity) simulations.

The mechanical behavior of the different Fe/Cu NMLs under uniaxial compression along the interface normal direction (corresponding to sample Z), as well as a shear compression in the sample YZ plane is compared for different Fe/Cu NMLs. As expected, the deformation response in the sample under normal compression is significantly different from that under the shear for all types of Fe/Cu NMLs studied, with earlier yielding observed under shear as compared to the normal compression. Figure 12 plots the dislocation density evolution for the different slip systems in the Cu, (a), and the Fe, (b), layers under normal compression for one of the four Fe/Cu NML microstructures with 400 nm layer thickness and a {1 1 2}/{1 1 2} interface relationship. It is interesting to see a similarity in plasticity mechanism for both the layers where a system that was inactive

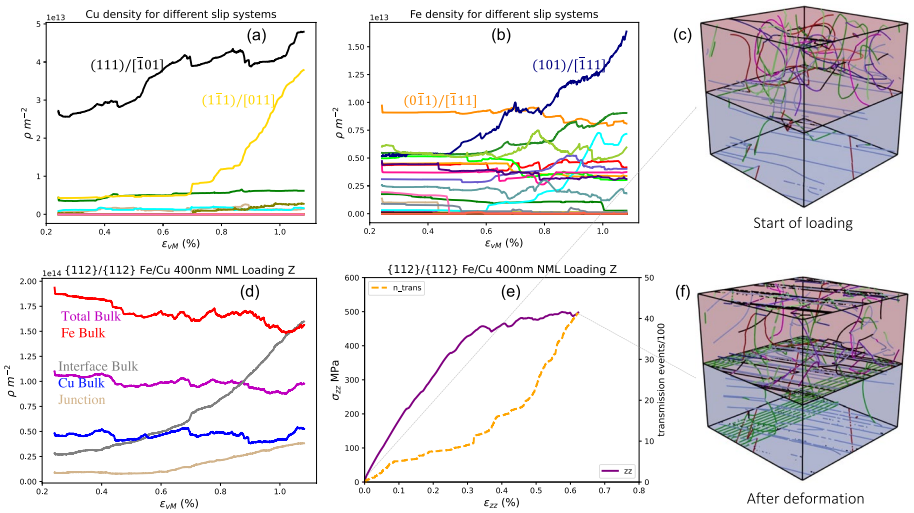


**Fig. 12** The dislocation density evolution for the individual slip systems in the Cu, (**a**), and the Fe, (**b**), under ND compression loading is plotted as a function of average von Mises strain for one of the 4 runs shown in Fig. 6, for a 400 nm thick Fe/Cu NML with a {1 1 2}/{1 1 2} interface. **d** plots the corresponding averaged dislocation density evolution in the bulk (magenta), interface (gray), Fe bulk (red), and Cu bulk (blue), along with the bulk junction density (tan). The macroscopic ND stress-strain response with the number of transmission events is also plotted in (**e**). The relaxed dislocation microstructure at the start of loading and the final deformed configuration are shown in (**c**) and (**f**), respectively, with different colored segments corresponding to the different slip systems as illustrated in Fig. 3

initially increases in activity ((1 $\bar{1}$ 1)/[$\bar{1}$ 0 1] for the Cu phase and (0 $\bar{1}$ 1)/[$\bar{1}$ 1 1] for the Fe phase) as the deformation proceeds. Sometimes, this process can result in suppression of an initially active system (as correlated via the decrease in their dislocation density). The average bulk dislocation density evolution in the Fe and the Cu layers along with that of the interface is also plotted in (c), where, clearly, the interface dislocation density increases significantly with deformation, while the bulk dislocation densities decreases for both layers. This is also evident from the exemplary dislocation microstructure shown for both the initial, (c), and the final configuration, (f) in Fig. 12. Overall, the average bulk junction density increases with deformation after a certain imposed strain indicating significant dislocation activity in the material.

A completely different plastic response is observed for shear loading, as shown in Fig. 13. Even though there is late activation of an initially inactive system (like before), there is also a significant suppression of the initial active systems for both Cu, (a), and the Fe, (b), phases. Additionally, the average bulk dislocation densities significantly drop with deformation suggesting annihilation of dislocations in the bulk. The drop in dislocation density is most significant for the softer Cu layer due to the easier and higher slip activity, as compared to the harder Fe layer. This eventually leads to exhaustion of the available slip activity in the Cu layer, causing the material to harden. Following this, a transmission event occurs from the Fe to the Cu layer that then increases the density in the Cu layer and accommodates subsequent plastic activity. The shear stress-strain curve also tends to have significant hardening and stress drops under the shear compression loading, as shown in Fig. 13e, where each stress drop corresponds to an event that accommodates high plastic activity. The first stress drop (at $\sim$ 0.25% strain) is due to a slip transmission event from the Fe to the Cu phase. Next, the material hardens due to lack of dislocations, and formation of dipoles that eventually frees and dissociates to accommodate plastic

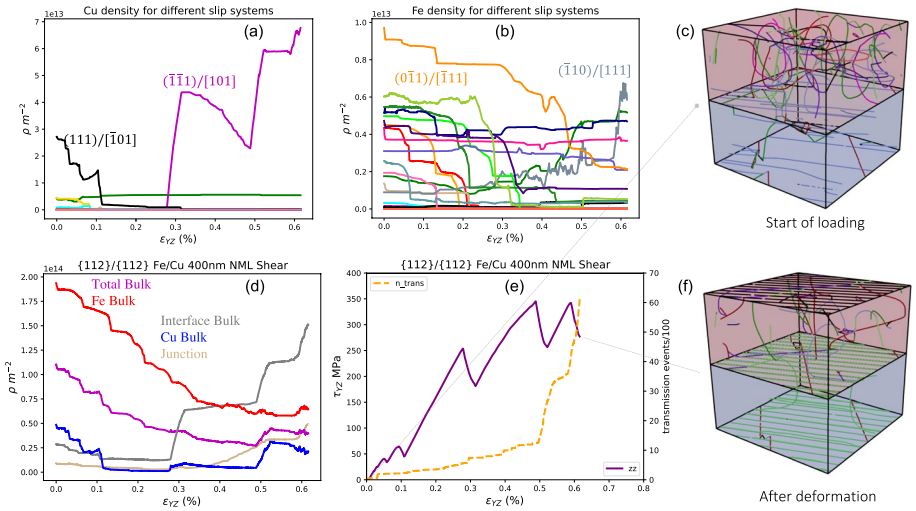


**Fig. 13** The dislocation density evolution for the individual slip systems in the Cu, (**a**), and the Fe, (**b**), under shear compression loading is plotted as a function of average von Mises strain for one of the 4 runs shown in Fig. 7, for a 400 nm thick Fe/Cu NML with a {1 1 2/1 1 2} interface. **d** plots the corresponding averaged dislocation density evolution in the bulk (magenta), interface (gray), Fe bulk (red), and Cu bulk (blue), along with the bulk junction density (tan). The macroscopic shear stress-strain response with the number of transmission events is also plotted in (**e**). The relaxed dislocation microstructure at the start of loading and the final deformed configuration are shown in (**c**) and (**f**), respectively

activity (second and the third stress drops in the shear stress-strain curves). The interface dislocation density also increases similar to the normal compression loading. However, a significant difference in mechanism being the high annihilation of dislocations observed under shear leads to limited bulk dislocations available to accommodate plasticity. This is also illustrated from the initial and final dislocation network configurations shown in (c) and (f) in Fig. 13. For both loading conditions bulk slip activity was observed to be via confined layer slip with threading dislocations gliding in their respective layers, as proposed previously for NMLs (Misra 2006; Misra et al. 2008, 2005).

Ultimately, the mechanical response under normal compression seems to be generally softer for the 400 nm thick NML as compared to the 200 nm thickness ((c) in Fig. 6), while a {1 1 0}/{1 1 1} interface appears to be "slightly" harder as compared to a {1 1 2}/{1 1 2} interface for the same layer thickness ((c) in Fig. 10). This qualitatively highlights the effect of both layer thickness and interface type on the overall mechanical response of the Fe/Cu NML. Additionally, the transmission propensity also seems to be influenced by both layer thickness and interface type, with, for example, a {1 1 0}/{1 1 1} interface tending to have significantly lower transmission events as compared to a {1 1 2}/{1 1 2} type interface. Presumably, as transmission propensity decreases for higher misorientation interfaces, these basic trends would continue. That is, even fewer dislocations in bulk with higher concentrations at interfaces and a strengthening effect on the initial yield point.

## Conclusion

This work aims to understand and model the effect of dislocation-interface interactions on internal residual stresses and overall mechanical response of ARB processed Fe/Cu NMLs. Specifically, we compared the effect of layer thickness and interface orientation relationship on the residual stresses generated in the initial relaxed microstructure post pre-strain-relaxation boundary condition, as well as the mechanical response under uniaxial and shear compression in the sample ND and ND-RD plane. Moreover, the slip transmission module developed in this work allows the model to capture various dislocation-interface interaction events, including dislocation transmission and dislocation-dislocation interactions across the two phases constituting the interface. The module, thus not only models a dynamically evolving interface, but also predicts its influence on the overall mechanical response and residual stresses for these NMLs. Critical findings through this work include:

- The pre-strain-relaxation boundary condition leads to different residual stresses in the Fe and the Cu layers whose magnitude is a strong function of layer thickness, with smaller layer thickness leading to higher residual stresses. The interface orientation relationship seems to have a negligible influence on the residual stress magnitude, but affects the nature of the stress.
- The transmission propensity is significantly affected by both layer thickness and interface orientation, both during microstructure generation and subsequent loading.
- As expected, the model indeed predicts a higher dislocation density for smaller layer thickness. Also, the relaxed configuration after the pre-strain-relaxation boundary

condition seems to generally have a higher dislocation density in the Fe layer as compared to the Cu layer irrespective of layer thickness or interface type.

- The model also predicts a comparable interface and bulk dislocation densities, with the former generally increasing with deformation.
- Finally, the DDD simulations predict a significant contrast in plastic mechanism as a function of loading direction for these NMLs, with the shear direction being much softer compared to normal direction compression.

In this study, we have restricted transmission events for cases with non-zero misorientation between the slip traces of the incoming and outgoing slip planes, as well as dislocation climb phenomena. Future work includes incorporating such effects and studying their role on the mechanical behavior of these NMLs. Also, the current framework neglects interactions between sessile dislocations from different phases, which would be considered in the subsequent work.

## Appendix A. Thermodynamic analysis of a single transmission event

Slip transmission is associated with an overall energy change of the system, and the unit transmission process can be considered to be two successive events: (i) first the transmission process of the incoming segment (in the incoming phase) to the transmitted segment (in the transmitted phase) and a residual segment should be energetically feasible at the interface; (ii) and second, there has to be enough driving force in the transmitted phase for the transmitted segment to glide into the bulk. In the DDD framework, both the events depend on the local stresses near the interface, which is a function of the dislocation configurations (interaction effects), the external driving forces, as well as the stiffness contrast between the incoming and the transmitted phases. Hence, there can be situations where the transmission event is energetically favorable, but there is not enough driving force for the transmitted segment to glide from the interface to the bulk, which would then lead to oscillating segments and illicit interactions, thus leading to creation of spurious dislocation segments and overall dynamics. Ideally, this can be eliminated by considering each transmission event and then running the dynamics to see its feasibility. If the dynamics does not allow an event then the transmission should not be allowed, and the next transmission event should be considered. Unfortunately, such a methodology is computationally infeasible since it increases the dynamics and short-range operations by the number of transmission events for each time step.

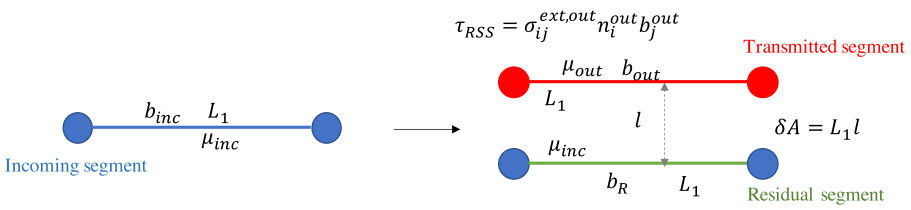


**Fig. 14** Schematic of unit transmission event where one incoming dislocation segment (blue; left) transmits to a residual (right; green) and a transmitted (right; red) segment. The spheres represents dislocation nodes, with the color scheme reflecting the phase allocation as per the proposed transmission algorithm in the DDD code

Thus, to avoid creation of a lot of such segments we perform a preliminary thermodynamic analysis for an ideal transmission of a single dislocation segment with length $L_1$, under an external stress $\sigma_{ext}$, as shown schematically in Fig. 14. As shown, the transmission leads to a residual segment and a transmitted segment separated by a distance $l$, with a sheared area, $\delta A$ of $L_1 l$. To determine the feasibility of the process, we use a line tension energy model and check whether the change in enthalpy decreases during the transmission event. Thus, the enthalpy of the incoming configuration is the energy due to line tension, $T$, which is the function of the character angle[5] of the dislocation segment, $\theta$, scaled by the segment length, $L_1$, as obtained from DeWit and Koehler (1959):

$$T = E_{el}(\theta) + \frac{d^2 E_{el}(\theta)}{d\theta^2} \tag{11}$$

with the elastic energy of the incoming segment, $E_{el,inc}$, given as, Weygand et al. (2002):

$$E_{el,inc} = L_1 \left( \frac{\mu_{inc} b_{inc}^2}{4\pi} \ln \frac{R}{r_0} \left[ \cos^2 \theta_{inc} + \frac{\sin^2 \theta_{inc}}{1 - \nu_{inc}} \right] \right) \tag{12}$$

with $\mu_{inc}, \nu_{inc}, b_{inc}, \theta_{inc}$ corresponding to the shear modulus, Poisson ratio, Burgers vector magnitude, and the character angle of the incoming dislocation. While $R, r_0$ relates to the outer cut-off and inner dislocation core radius, respectively. Similarly, the enthalpy of the transmitted configuration includes the energy from both the transmitted, $E_{el,out}$, and the residual segments, $E_{el,res}$, as well as the work done by the external force, $W_{ext}$, to shear the transmitted segment by an area $\delta A$, as shown in the schematic Fig. 14.

$$E_{el,out} = L_1 \left( \frac{\mu_{out} b_{out}^2}{4\pi} \ln \frac{R}{r_0} \left[ \cos^2 \theta_{out} + \frac{\sin^2 \theta_{out}}{1 - \nu_{out}} \right] \right) \tag{13}$$

$$E_{el,res} = L_1 \left( \frac{\mu_{res} b_{res}^2}{4\pi} \ln \frac{R}{r_0} \left[ \cos^2 \theta_{res} + \frac{\sin^2 \theta_{res}}{1 - \nu_{res}} \right] \right) \tag{14}$$

$$W_{ext} = \tau_{RSS} b_{out} \delta A = \tau_{RSS} b_{out} L_1 l \tag{15}$$

Moreover, the transmitted configuration will also have an interaction energy, $E_{int}$, between the transmitted segment and the residual segment, which will also influence the overall energy of the configuration. In this work, we use the simplified form of the interaction energy as used in Capolungo and Beyerlein (2008),

$$E_{int} = -L_1 \mu_{inc} \frac{(\boldsymbol{b_{inc}} \cdot \boldsymbol{\xi})(\boldsymbol{b_{res}} \cdot \boldsymbol{\xi})}{2\pi} \ln \frac{l}{r_0} - L_1 \mu_{inc} \frac{(\boldsymbol{b_{inc}} \times \boldsymbol{\xi}) \cdot (\boldsymbol{b_{res}} \times \boldsymbol{\xi})}{2\pi (1 - \nu_{inc})} \ln \frac{l}{r_0} - L_1 \mu_{inc} \frac{[(\boldsymbol{b_{inc}} \times \boldsymbol{\xi}) \cdot \boldsymbol{l}] \cdot [(\boldsymbol{b_{res}} \times \boldsymbol{\xi}) \cdot \boldsymbol{l}]}{2\pi (1 - \nu_{inc}) l^2} \tag{16}$$

where, $\boldsymbol{\xi}$ is the trace of the incoming and transmitting slip planes at the interface, and $\boldsymbol{l}$ is the distance vector between the residual and the transmitted segment with a magnitude

[5] angle between the Burgers vector and dislocation line direction

corresponding to the distance between the two segments, $l$. Hence, the energy of the system now becomes a function of the external applied shear stress, $\tau_{RSS}$, as well as the distance between the two segments, $l$. Figure 15 plots the enthalpy change per unit dislocation line length for a particular set of slip systems in the fcc-Cu ((1 1 1)/[$\bar{1}$ 0 1]) and bcc-Fe ((0 1 1)/[1 $\bar{1}$ 1]) phases, against relative distance between the residual and transmitted segments normalized by the incoming dislocation Burgers vector, and having a {1 1 2}/{1 1 2} interface. Clearly, transmission from Fe to Cu is readily feasible ($\Delta H$ is negative), while that from Cu to Fe appears to be infeasible for these materials under realistic layer thicknesses and external driving forces. This also aligns with atomistic simulations, where the Koehler forces, due to the stiffness contrast in the material, will push the dislocation from the harder phase towards the softer phase. We incorporated such effect by disallowing any transmission from the Cu to the Fe phase in the DDD simulations.

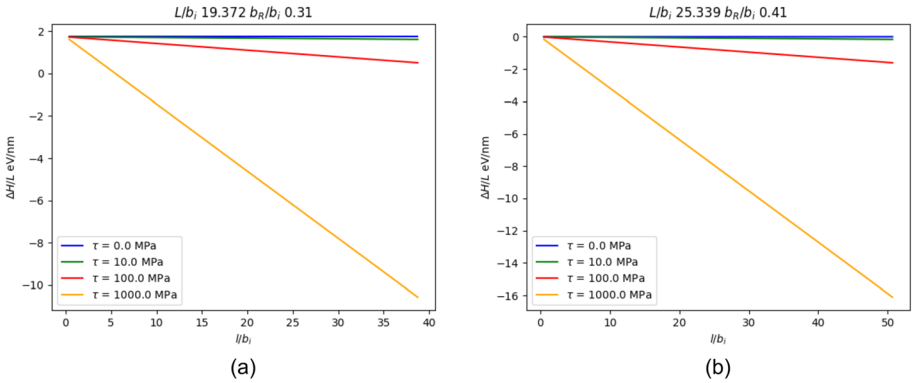


**Fig. 15** Variation of enthalpy change per unit length of the dislocation segment upon a transmission event from the fcc to the bcc phase, (**a**), and vice-versa, (**b**), as a function of distance between the transmitted and residual segments normalized by the incoming Burgers vector, for different external applied shear stress, $\tau_{RSS}$. A given transmission configuration (specific incoming and transmitting slip systems) is considered for both the cases, for a {1 1 2}/{1 1 2} Fe/Cu NML structure. The analytical results indicate that slip transmission from fcc to bcc phase is realistically infeasible

**Acknowledgements**
AC acknowledges Darshan Bamney from Los Alamos National Laboratory for algorithmic discussions with the DDD code, and Douglas E Spearot from University of Florida for valuable insight on interface effects.

**Authors' contributions**
A.C Performed simulations, conceptualized the problem. All authors reviewed the manuscript, edited the manuscript, derived the modeling framework, verified results.

**Funding**
This work was funded by the Laboratory Directed Research and Development (LDRD) program through 20200182DR at Los Alamos National Laboratory.

**Availability of data and materials**
The data in this paper is available from the corresponding author upon reasonable request.

## Declarations

**Ethics approval and consent to participate**
Not applicable.

**Consent for publication**
Not applicable.

**Competing interests**
The authors declare no competing interests.

Received: 21 June 2023 Accepted: 19 January 2024
Published online: 27 February 2024

**References**

F. Akasheh, H.M. Zbib, J.P. Hirth, R.G. Hoagland, A. Misra, Dislocation dynamics analysis of dislocation intersections in nanoscale metallic multilayered composites. J. Appl. Phys. **101**(8) (2007). https://doi.org/10.1063/1.2721093
F. Akasheh, H.M. Zbib, J.P. Hirth, R.G. Hoagland, A. Misra, Interactions between glide dislocations and parallel interfacial dislocations in nanoscale strained layers. J. Appl. Phys. **102**(3), 034314 (2007). https://doi.org/10.1063/1.2757082. https://aip.scitation.org/doi/10.1063/1.2757082
P.M. Anderson, C. Li, Hall-Petch relations for multilayered materials. Nanostruct. Mater. **5**(3), 349–362 (1995). https://doi.org/10.1016/0965-9773(95)00250-I
P.M. Anderson, T. Foecke, P.M. Hazzledine, Dislocation-based deformation mechanisms in metallic nanolaminates. MRS Bulletin. **24**(2), 27–33 (1999). https://doi.org/10.1557/S0883769400051514
D.V. Bachurin, D. Weygand, P. Gumbsch, Dislocation-grain boundary interaction in ⟨111⟩ textured thin metal films. Acta Mater. **58**(16), 5232–5241 (2010). https://doi.org/10.1016/j.actamat.2010.05.037
D. Bamney, R. Reyes, L. Capolungo, D.E. Spearot, Disclination-dislocation based model for grain boundary stress field evolution due to slip transmission history and influence on subsequent dislocation transmission. J. Mech. Phys. Solids. **165** (2022). https://doi.org/10.1016/j.jmps.2022.104920
D. Bamney, L. Capolungo, D.E. Spearot, Role of equilibrium and non-equilibrium grain boundary stress fields on dislocation transmission. J. Mater. Res. **36**, 2687–2704 (2021)
N. Bertin, Connecting discrete and continuum dislocation mechanics: a non-singular spectral framework. Int. J. Plast. **122**, 268–284 (2019). https://doi.org/10.1016/j.ijplas.2018.12.006. arXiv:1804.00803
N. Bertin, M.V. Upadhyay, C. Pradalier, L. Capolungo, A FFT-based formulation for efficient mechanical fields computation in isotropic and anisotropic periodic discrete dislocation dynamics. Model. Simul. Mater. Sci. Eng. **23**(6) (2015). https://doi.org/10.1088/0965-0393/23/6/065009
N. Bertin, L. Capolungo, A FFT-based formulation for discrete dislocation dynamics in heterogeneous media. J. Comput. Phys. **355**, 366–384 (2018). https://doi.org/10.1016/j.jcp.2017.11.020
I.J. Beyerlein, A. Hunter, Understanding dislocation mechanics at the mesoscale using phase field dislocation dynamics (2016). https://doi.org/10.1098/rsta.2015.0166. https://dx.doi.org/10.1098/rsta.2015.0166
I.J. Beyerlein, N.A. Mara, J. Wang, J.S. Carpenter, S.J. Zheng, W.Z. Han, R.F. Zhang, K. Kang, T. Nizolek, T.M. Pollock, Structure-property-functionality of bimetal interfaces. JOM **64**(10), 1192–1207 (2012). https://doi.org/10.1007/s11837-012-0431-0. https://link.springer.com/article/10.1007/s11837-012-0431-0
I.J. Beyerlein, N.A. Mara, J.S. Carpenter, T. Nizolek, W.M. Mook, T.A. Wynn, R.J. McCabe, J.R. Mayeur, K. Kang, S. Zheng, J. Wang, T.M. Pollock, Interface-driven microstructure development and ultra high strength of bulk nanostructured Cu-Nb multilayers fabricated by severe plastic deformation. J. Mater. Res. **28**(13), 1799–1812 (2013). https://doi.org/10.1557/jmr.2013.21. https://link.springer.com/article/10.1557/jmr.2013.21
N.B. Burbery, G. Po, R. Das, N. Ghoniem, W.G. Ferguson, Dislocation dynamics in polycrystals with atomistic-informed mechanisms of dislocation - grain boundary interactions. J. Micromech. Mol. Phys. **2**(1), 1750003 (2017). https://doi.org/10.1142/S2424913017500035. https://www.worldscientific.com
Z.H. Cao, Y.P. Cai, C. Sun, Y.J. Ma, M.Z. Wei, Q. Li, H.M. Lu, H. Wang, X. Zhang, X.K. Meng, Tailoring strength and plasticity of Ag/Nb nanolaminates via intrinsic microstructure and extrinsic dimension. Int. J. Plast. **113**, 145–157 (2019). https://doi.org/10.1016/j.ijplas.2018.09.012
L. Capolungo, I.J. Beyerlein, Nucleation and stability of twins in hcp metals. Phys. Rev. B Condens. Matter Mater. Phys. **78**(2), 024117 (2008). https://doi.org/10.1103/PhysRevB.78.024117. https://journals.aps.org/prb/abstract/10.1103/PhysRevB.78.024117
L. Capolungo, V. Taupin, GD3: generalized discrete defect dynamics. Mater. Theory. **3**(1), 1–21 (2019). https://doi.org/10.1186/s41313-018-0013-9. https://link.springer.com/articles/10.1186/s41313-018-0013-9; https://link.springer.com/article/10.1186/s41313-018-0013-9
J.S. Carpenter, R.J. McCabe, S.J. Zheng, T.A. Wynn, N.A. Mara, I.J. Beyerlein, in *Metallurgical and Materials Transactions A: Physical Metallurgy and Materials Science*, vol. 45, Processing parameter influence on texture and microstructural evolution in cu-nb multilayer composites fabricated via accumulative roll bonding (Springer Boston, 2014), pp. 2192–2208. https://doi.org/10.1007/s11661-013-2162-4. https://link.springer.com/article/10.1007/s11661-013-2162-4
J. Carpenter, S. Zheng, R. Zhang, S. Vogel, I. Beyerlein, N. Mara, Thermal stability of Cu–Nb nanolamellar composites fabricated via accumulative roll bonding. Phil. Mag. **93**(7), 718–735 (2013). https://doi.org/10.1080/14786435.2012.731527. https://www.tandfonline.com/doi/abs/10.1080/14786435.2012.731527
A. Chakraborty, A. Hunter, L. Capolungo, Effect of microstructure, layer thickness, and interface behavior on the plasticity of accumulative roll bonded nanometallic laminates using dislocation dynamics simulations. J. Mater. Res. **36**(13), 2715–2728 (2021). https://doi.org/10.1557/s43578-021-00144-2. https://www.mrs.org/jmr
T. Chen, R. Yuan, I.J. Beyerlein, C. Zhou, Predicting the size scaling in strength of nanolayered materials by a discrete slip crystal plasticity model. Int. J. Plast. **124**, 247–260 (2020). https://doi.org/10.1016/j.ijplas.2019.08.016
J. Cho, J.C. Crone, A. Arsenlis, S. Aubry, Dislocation dynamics in polycrystalline materials. Model. Simul. Mater. Sci. Eng. **28**(3), 035009 (2020). https://doi.org/10.1088/1361-651X/ab6da8
H.J. Chu, J. Wang, I.J. Beyerlein, E. Pan, Dislocation models of interfacial shearing induced by an approaching lattice glide dislocation. Int. J. Plast. **41**, 1–13 (2013). https://doi.org/10.1016/j.ijplas.2012.08.005

M.J. Demkowicz, R.G. Hoagland, J.P. Hirth, Interface structure and radiation damage resistance in Cu-Nb multilayer nanocomposites. Phys. Rev. Lett **100**(13), 136102 (2008). https://doi.org/10.1103/PhysRevLett.100.136102
M.J. Demkowicz, P. Bellon, B.D. Wirth, Atomic-scale design of radiation-tolerant nanocomposites. MRS Bull. **35**(12), 992–998 (2010). https://doi.org/10.1557/mrs2010.704
G. DeWit, J.S. Koehler, Interaction of dislocations with an applied stress in anisotropic crystals. Phys. Rev. **116**(5), 1113–1120 (1959). https://doi.org/10.1103/PhysRev.116.1113. https://journals.aps.org/pr/abstract/10.1103/PhysRev.116.1113
L. Dupuy, M.C. Fivel, A study of dislocation junctions in FCC metals by an orientation dependent line tension model. Acta Mater. **50**(19), 4873–4885 (2002). https://doi.org/10.1016/S1359-6454(02)00356-7
M. Eizadjou, A. Kazemi Talachi, H. Danesh Manesh, H. Shakur Shahabi, K. Janghorban, Investigation of structure and mechanical properties of multi-layered Al/Cu composite produced by accumulative roll bonding (ARB) process. Compos. Sci. Technol. **68**(9), 2003–2009 (2008). https://doi.org/10.1016/j.compscitech.2008.02.029
J.A. El-Awady, H. Fan, A.M. Hussein, in *Springer Series in Materials Science*, vol. 245, Advances in discrete dislocation dynamics modeling of size-affected plasticity (Springer Verlag, 2016), pp. 337–371. https://doi.org/10.1007/978-3-319-33480-6_11. https://link.springer.com/chapter/10.1007/978-3-319-33480-6_11
L.H. Friedman, D.C. Chrzan, Scaling Theory of the Hall-Petch Relation for Multilayers. Phys. Rev. Lett. **81**(13), 2715–2718 (1998). https://doi.org/10.1103/PhysRevLett.81.2715. https://journals.aps.org/prl/abstract/10.1103/PhysRevLett.81.2715
L. Ghalandari, M.M. Moshksar, High-strength and high-conductive Cu/Ag multilayer produced by ARB. J. Alloys Compd. **506**(1), 172–178 (2010). https://doi.org/10.1016/j.jallcom.2010.06.172
N. Ghoniem, S. Tong, L. Sun, Parametric dislocation dynamics: A thermodynamics-based approach to investigations of mesoscopic plastic deformation. Phys. Rev. B Condens. Matter Mater. Phys. **61**(2), 913–927 (2000). https://doi.org/10.1103/PhysRevB.61.913. https://journals.aps.org/prb/abstract/10.1103/PhysRevB.61.913
R.G. Hoagland, T.E. Mitchell, J.P. Hirth, H. Kung, On the strengthening effects of interfaces in multilayer fee metallic composites. Philos. Mag. A Phys. Condens. Matter Struct. Defects Mech. Prop. **82**(4), 643–664 (2002). https://doi.org/10.1080/01418610208243194. https://www.tandfonline.com/action/journalInformation?journalCode=tphm20
R.G. Hoagland, R.J. Kurtz, C.H. Henager, Slip resistance of interfaces and the strength of metallic multilayer composites. Scr. Mater. **50**(6), 775–779 (2004). https://doi.org/10.1016/j.scriptamat.2003.11.059
R.G. Hoagland, J.P. Hirth, A. Misra, On the role of weak interfaces in blocking slip in nanoscale layered composites. Philos. Mag. **86**(23), 3537–3558 (2006). https://doi.org/10.1080/14786430600669790
A. Hunter, I.J. Beyerlein, Stacking fault emission from grain boundaries: Material dependencies and grain size effects. Mater. Sci. Eng. A. **600**, 200–210 (2014). https://doi.org/10.1016/j.msea.2014.02.030
A. Hunter, R.F. Zhang, I.J. Beyerlein, The core structure of dislocations and their relationship to the material $\gamma$-surface. J. Appl. Phys. **115**(13), 134314 (2014). https://doi.org/10.1063/1.4870462. https://aip.scitation.org/doi/10.1063/1.4870462
D. Josell, D. Van Heerden, D. Read, J. Bonevich, D. Shechtman, Tensile testing low density multilayers: Aluminum/titanium. J. Mater. Res. **13**(10), 2902–2909 (1998). https://doi.org/10.1557/JMR.1998.0397. https://link.springer.com/article/10.1557/JMR.1998.0397
J.S. Koehler, Attempt to design a strong solid. Phys. Rev. B **2**(2), 547–551 (1970). https://doi.org/10.1103/PhysRevB.2.547. https://journals.aps.org/prb/abstract/10.1103/PhysRevB.2.547
A.A. Kohnert, L. Capolungo, The kinetics of static recovery by dislocation climb. NPJ Comput. Mater. **8**(1) (2022). https://doi.org/10.1038/s41524-022-00790-y
A.A. Kohnert, L. Capolungo, Spectral discrete dislocation dynamics with anisotropic short range interactions. Comput. Mater. Sci. **189**, 110243 (2021). https://doi.org/10.1016/j.commatsci.2020.110243
L.P. Kubin, *Dislocations, Mesoscale Simulations and Plastic Flow* (Oxford University Press, 2013)
F. Kümmel, B. Diepold, K.F. Sauer, C. Schunk, A. Prakash, H.W. Höppel, M. Göken, High lightweight potential of ultrafine-grained aluminum/steel laminated metal composites produced by accumulative roll bonding. Adv. Eng. Mater. **21**(1), 1800286 (2019). https://doi.org/10.1002/adem.201800286. https://onlinelibrary.wiley.com/doi/abs/10.1002/adem.201800286; https://onlinelibrary.wiley.com/doi/pdf/10.1002/adem.201800286
R.A. Lebensohn, A.K. Kanjarla, P. Eisenlohr, An elasto-viscoplastic formulation based on fast Fourier transforms for the prediction of micromechanical fields in polycrystalline materials. Int. J. Plast. **32–33**, 59–69 (2012). https://doi.org/10.1016/j.ijplas.2011.12.005
T.C. Lee, I.M. Robertson, H.K. Birnbaum, Prediction of slip transfer mechanisms across grain boundaries. Scr. Metall. **23**(5), 799–803 (1989). https://doi.org/10.1016/0036-9748(89)90534-6
L. Lei, J.L. Marin, M. Koslowski, Phase-field modeling of defect nucleation and propagation in domains with material inhomogeneities. Model. Simul. Mater. Sci. Eng. **21**(2), 025009 (2013). https://doi.org/10.1088/0965-0393/21/2/025009. https://iopscience.iop.org/article/10.1088/0965-0393/21/2/025009; https://iopscience.iop.org/article/10.1088/0965-0393/21/2/025009/meta
N. Li, J. Wang, A. Misra, J.Y. Huang, Direct observations of confined layer slip in cu/nb multilayers. Microsc Microanalisys. **5**(18) (2012). https://doi.org/10.1017/S143192761200133X
Z. Li, C. Hou, M. Huang, C. Ouyang, Strengthening mechanism in micro-polycrystals with penetrable grain boundaries by discrete dislocation dynamics simulation and Hall-Petch effect. Comput. Mater. Sci. **46**(4), 1124–1134 (2009). https://doi.org/10.1016/j.commatsci.2009.05.021
L.C. Lim, R. Raj, Continuity of slip screw and mixed crystal dislocations across bicrystals of nickel at 573 K. Acta Metall. **33**(8), 1577–1583 (1985). https://doi.org/10.1016/0001-6160(85)90057-4
J.D. Livingston, B. Chalmers, Multiple slip in bicrystal deformation. Acta Metall. **5**(6), 322–327 (1957). https://doi.org/10.1016/0001-6160(57)90044-5
A. Ma, F. Roters, D. Raabe, On the consideration of interactions between dislocations and grain boundaries in crystal plasticity finite element modeling - Theory, experiments, and simulations. Acta Mater. **54**(8), 2181–2194 (2006). https://doi.org/10.1016/j.actamat.2006.01.004
N.A. Mara, D. Bhattacharyya, R.G. Hoagland, A. Misra, Tensile behavior of 40 nm Cu/Nb nanoscale multilayers. Scr. Mater. **58**(10), 874–877 (2008). https://doi.org/10.1016/j.scriptamat.2008.01.005

J.R. Mayeur, D.L. McDowell, A three-dimensional crystal plasticity model for duplex Ti-6Al-4V. Int. J. Plast. **23**(9), 1457–1485 (2007). https://doi.org/10.1016/j.ijplas.2006.11.006
J.R. Mayeur, I.J. Beyerlein, C.A. Bronkhorst, H.M. Mourad, B.L. Hansen, A crystal plasticity study of heterophase interface character stability of Cu/Nb bicrystals. Int. J. Plast. **48**, 72–91 (2013). https://doi.org/10.1016/j.ijplas.2013.02.006
S. Menezes, D.P. Anderson, Wavelength-Property Correlation in Electrodeposited Ultrastructured Cu-Ni Multilayers. J. Electrochem. Soc. **137**(2), 440–444 (1990). https://doi.org/10.1149/1.2086459. https://iopscience.iop.org/article/10.1149/1.2086459; https://iopscience.iop.org/article/10.1149/1.2086459/meta
M.A. Meyers, A. Mishra, D.J. Benson, Mechanical properties of nanocrystalline materials (2006). https://doi.org/10.1016/j.pmatsci.2005.08.003
G. Min, J.M. Lee, S.B. Kang, H.W. Kim, Evolution of microstructure for multilayered Al/Ni composites by accumulative roll bonding process. Mater. Lett. **60**(27), 3255–3259 (2006). https://doi.org/10.1016/j.matlet.2006.03.001
A. Misra, in *Nanostructure Control of Materials*, Mechanical behavior of metallic nanolaminates (Elsevier, 2006), pp. 146–176. https://doi.org/10.1533/9781845691189.146
A. Misra, R. Gibala, Slip transfer and dislocation nucleation processes in multiphase ordered Ni-Fe-Al alloys. Metall. and Mater. Trans. A Phys. Metall. Mater. Sci. **30**(4), 991–1001 (1999). https://doi.org/10.1007/s11661-999-0152-3. https://link.springer.com/article/10.1007/s11661-999-0152-3
A. Misra, J.P. Hirth, H. Kunc, Single-dislocation-based strengthening mechanisms in nanoscale metallic multilayers. Phil. Mag. A Phys. Condens. Matter Struct. Defects Mech. Prop. **82**(16), 2935–2951 (2002). https://doi.org/10.1080/01418610208239626. https://www.tandfonline.com/doi/abs/10.1080/01418610208239626
A. Misra, R. Hoagland, H. Kung ‡, Thermal stability of self-supported nanolayered Cu/Nb films. Philos. Mag. **84**(10), 1021–1028 (2004). https://doi.org/10.1080/14786430310001659480. http://www.tandfonline.com/doi/abs/10.1080/14786430310001659480
A. Misra, R.G. Hoagland, Effects of elevated temperature annealing on the structure and hardness of copper/niobium nanolayered films. J. Mater. Res. **20**(8), 2046–2054 (2005). https://doi.org/10.1557/JMR.2005.0250
A. Misra, R.G. Hoagland, Plastic flow stability of metallic nanolaminate composites. J. Mater. Sci. **42**(5), 1765–1771 (2007). https://doi.org/10.1007/s10853-006-0895-9
A. Misra, H. Kung, Deformation behavior of nanostructured metallic multilayers. Adv. Eng. Mater. **3**(4), 217–222 (2001).
A. Misra, J.P. Hirth, R.G. Hoagland, Length-scale-dependent deformation mechanisms in incoherent metallic multilayered composites. Acta Mater. **53**(18), 4817–4824 (2005). https://doi.org/10.1016/j.actamat.2005.06.025
A. Misra, M.J. Demkowicz, J. Wang, R.G. Hoagland, The multiscale modeling of plastic deformation in metallic nanolayered composites (2008). https://doi.org/10.1007/s11837-008-0047-6. https://www.tms.org/jom.html
H. Moulinec, P. Suquet, A numerical method for computing the overall response of nonlinear composites with complex microstructure. Comput. Methods Appl. Mech. Eng. **157**(1–2), 69–94 (1998). https://doi.org/10.1016/S0045-7825(97)00218-1
H.M. Mourad, K. Garikipati, Advances in the numerical treatment of grain-boundary migration: Coupling with mass transport and mechanics. Comput. Methods Appl. Mech. Eng. **196**(1–3), 595–607 (2006). https://doi.org/10.1016/j.cma.2006.06.005
T. Nizolek, N.A. Mara, I.J. Beyerlein, J.T. Avallone, T.M. Pollock, Enhanced Plasticity via Kinking in Cubic Metallic Nanolaminates. Adv. Eng. Mater. **17**(6), 781–785 (2015). https://doi.org/10.1002/adem.201400324. https://doi.wiley.com/10.1002/adem.201400324
T. Nizolek, I.J. Beyerlein, N.A. Mara, J.T. Avallone, T.M. Pollock, Tensile behavior and flow stress anisotropy of accumulative roll bonded Cu-Nb nanolaminates. Appl. Phys. Lett. **108**(5), 051903 (2016). https://doi.org/10.1063/1.4941043. https://aip.scitation.org/doi/10.1063/1.4941043
E.S. Pacheco, T. Mura, Interaction between a screw dislocation and a bimetallic interface. J. Mech. Phys. Solids. **17**(3), 163–170 (1969). https://doi.org/10.1016/0022-5096(69)90030-1
C.S. Pande, R.A. Masumura, R.W. Armstrong, Pile-up based hall-petch relation for nanoscale materials. Nanostruct. Mater. **2**(3), 323–331 (1993). https://doi.org/10.1016/0965-9773(93)90159-9
S. Papanikolaou, M. Tzimas, A.C.E. Reid, S.A. Langer, Spatial strain correlations, machine learning, and deformation history in crystal plasticity. Phys. Rev. E **99**, 053,003 (2019). https://doi.org/10.1103/PhysRevE.99.053003. https://link.aps.org/doi/10.1103/PhysRevE.99.053003
P.M. Pohl, M. Kuglstatter, M. Göken, H.W. Höppel, Quantifying co-deformation effects in metallic laminates by loading;unloading;reloading tensile tests. Metals. **13**(6) (2023). https://doi.org/10.3390/met13061049. https://www.mdpi.com/2075-4701/13/6/1049
I. Radchenko, H.P. Anwarali, S.K. Tippabhotla, A.S. Budiman, Effects of interface shear strength during failure of semicoherent Metal–Metal nanolaminates: An example of accumulative roll-bonded Cu/Nb. Acta Mater. **156**, 125–135 (2018). https://doi.org/10.1016/j.actamat.2018.06.023
S.I. Rao, P.M. Hazzledine, Atomistic simulations of dislocation-interface interactions in the Cu-Ni multilayer system. Philos. Mag. A Phys. Condens. Matter Struct. Defects Mech. Prop. **80**(9), 2011–2040 (2000). https://doi.org/10.1080/01418610008212148. https://www.tandfonline.com/action/journalInformation?journalCode=tpha20
I.M. Robertson, T.C. Lee, P. Rozenak, G.M. Bond, H.K. Birnbaum, Dynamic observations of the transfer of slip across a grain boundary. Ultramicroscopy. **30**(1–2), 70–75 (1989). https://doi.org/10.1016/0304-3991(89)90174-5
F. Roters, P. Eisenlohr, L. Hantcherli, D.D. Tjahjanto, T.R. Bieler, D. Raabe, Overview of constitutive laws, kinematics, homogenization and multiscale methods in crystal plasticity finite-element modeling: Theory, experiments, applications. Acta Mater. **58**(4), 1152–1211 (2010). https://doi.org/10.1016/j.actamat.2009.10.058
M.D. Sangid, T. Ezaz, H. Sehitoglu, I.M. Robertson, Energy of slip transmission and nucleation at grain boundaries. Acta Mater. **59**(1), 283–296 (2011). https://doi.org/10.1016/j.actamat.2010.09.032
S. Shao, A. Misra, H. Huang, J. Wang, Micro-scale modeling of interface-dominated mechanical behavior. J. Mater. Sci. **53**(8), 5546–5561 (2018). https://doi.org/10.1007/s10853-017-1662-9
M.A. Shehadeh, G. Lu, S. Banerjee, N. Kioussis, N. Ghoniem, Dislocation transmission across the Cu/Ni interface: a hybrid atomistic–continuum study. Philos. Mag. **87**(10), 1513–1529 (2007). https://doi.org/10.1080/14786430601055379. https://www.tandfonline.com/doi/abs/10.1080/14786430601055379

R.B. Sills, W.P. Kuykendall, A. Aghaei, W. Cai, in *Springer Series in Materials Science*, vol. 245, Fundamentals of dislocation dynamics simulations (Springer Verlag, 2016), pp. 53–87. https://doi.org/10.1007/978-3-319-33480-6_2. https://link.springer.com/chapter/10.1007/978-3-319-33480-6_2

C. Sobie, M.G. McPhie, L. Capolungo, M. Cherkaoui, The effect of interfaces on the mechanical behaviour of multilayered metallic laminates. Model. Simul. Mater. Sci. Eng. **22**(4) (2014). https://doi.org/10.1088/0965-0393/22/4/045007

M. Stricker, J. Gagel, S. Schmitt, K. Schulz, D. Weygand, P. Gumbsch, On slip transmission and grain boundary yielding. Meccanica **51**(2), 271–278 (2016). https://doi.org/10.1007/s11012-015-0192-2. https://link.springer.com/article/10.1007/s11012-015-0192-2

D.M. Tench, J.T. White, Tensile Properties of Nanostructured Ni-Cu Multilayered Materials Prepared by Electrodeposition. J. Electrochem. Soc. **138**(12), 3757–3758 (1991). https://doi.org/10.1149/1.2085495. https://iopscience.iop.org/article/10.1149/1.2085495; https://iopscience.iop.org/article/10.1149/1.2085495/meta

P.R. Van Beers, G.J. McShane, V.G. Kouznetsova, M.G. Geers, Grain boundary interface mechanics in strain gradient crystal plasticity. J. Mech. Phys. Solids. **61**(12), 2659–2679 (2013). https://doi.org/10.1016/j.jmps.2013.08.011

J. Wang, A. Misra, An overview of interface-dominated deformation mechanisms in metallic multilayers (2011). https://doi.org/10.1016/j.cossms.2010.09.002

Z. Wang, N. Ghoniem, S. Swaminarayan, R. LeSar, A parallel algorithm for 3D dislocation dynamics. J. Comput. Phys. **219**(2), 608–621 (2006). https://doi.org/10.1016/j.jcp.2006.04.005

J. Wang, R.G. Hoagland, J.P. Hirth, A. Misra, Atomistic modeling of the interaction of glide dislocations with "weak" interfaces. Acta Mater. **56**(19), 5685–5693 (2008). https://doi.org/10.1016/j.actamat.2008.07.041

J. Wang, A. Misra, R.G. Hoagland, J.P. Hirth, Slip transmission across fcc/bcc interfaces with varying interface shear strengths. Acta Mater. **60**(4), 1503–1513 (2012). https://doi.org/10.1016/j.actamat.2011.11.047

J. Wang, C. Zhou, I.J. Beyerlein, S. Shao, Modeling interface-dominated mechanical behavior of nanolayered crystalline composites (2014). https://doi.org/10.1007/s11837-013-0808-8. https://link.springer.com/article/10.1007/s11837-013-0808-8

D.A. Wei, M. Zaiser, Z. Feng, G. Kang, H. Fan, X. Zhang, Effects of twin boundary orientation on plasticity of bicrystalline copper micropillars: a discrete dislocation dynamics simulation study. Acta Mater. **176**, 289–296 (2019). https://doi.org/10.1016/j.actamat.2019.07.007

E. Werner, W. Prantl, Slip transfer across grain and phase boundaries. Acta Metall. Mater. **38**(3), 533–537 (1990). https://doi.org/10.1016/0956-7151(90)90159-E

D. Weygand, L.H. Friedman, E. Van Der Giessen, A. Needleman, Aspects of boundary-value problem solutions with three-dimensional dislocation dynamics. Model. Simul. Mater. Sci. Eng. **10**(4), 437–468 (2002). https://doi.org/10.1088/0965-0393/10/4/306. https://iopscience.iop.org/article/10.1088/0965-0393/10/4/306; https://iopscience.iop.org/article/10.1088/0965-0393/10/4/306/meta

K. Wu, H. Chang, E. Maawad, W.M. Gan, H.G. Brokmeier, M.Y. Zheng, Microstructure and mechanical properties of the Mg/Al laminated composite fabricated by accumulative roll bonding (ARB). Mater. Sci. Eng. A **527**(13–14), 3073–3078 (2010). https://doi.org/10.1016/j.msea.2010.02.001

D. Yang, P. Cizek, P. Hodgson, C. Wen, Ultrafine equiaxed-grain Ti/Al composite produced by accumulative roll bonding. Scr. Mater. **62**(5), 321–324 (2010). https://doi.org/10.1016/j.scriptamat.2009.11.036

H.M. Zbib, C.T. Overman, F. Akasheh, D. Bahr, Analysis of plastic deformation in nanoscale metallic multilayers with coherent and incoherent interfaces. Int. J. Plast. **27**(10), 1618–1639 (2011). https://doi.org/10.1016/j.ijplas.2011.03.006

Y. Zeng, A. Hunter, I.J. Beyerlein, M. Koslowski, A phase field dislocation dynamics model for a bicrystal interface system: An investigation into dislocation slip transmission across cube-on-cube interfaces. Int. J. Plast. **79**, 293–313 (2016). https://doi.org/10.1016/j.ijplas.2015.09.001

Y. Zhang, J.G. Gigax, T.J. Nizolek, J.S. Carpenter, M.M. Schneider, N. Li, L. Capolungo, R.J. McCabe, Tensile and failure behaviors of cu/nb nanolaminates: the effects of loading direction, layer thickness, and annealing. Acta Mater. **240**, 118346 (2022). https://doi.org/10.1016/j.actamat.2022.118346. https://www.sciencedirect.com/science/article/pii/S135964542200725X

J.Y. Zhang, K. Wu, L.Y. Zhang, Y.Q. Wang, G. Liu, J. Sun, Unraveling the correlation between Hall-Petch slope and peak hardness in metallic nanolaminates. Int. J. Plast. **96**, 120–134 (2017). https://doi.org/10.1016/j.ijplas.2017.04.020

Z. Zhang, C. Shao, S. Wang, X. Luo, K. Zheng, H.M. Urbassek, Interaction of Dislocations and Interfaces in Crystalline Heterostructures: A Review of Atomistic Studies. Crystals. **9**(11), 584 (2019). https://doi.org/10.3390/cryst9110584. https://www.mdpi.com/2073-4352/9/11/584

X. Zhang, S. Lu, B. Zhang, X. Tian, Q. Kan, G. Kang, Dislocation - grain boundary interaction-based discrete dislocation dynamics modeling and its application to bicrystals with different misorientations. Acta Mater. **202**, 88–98 (2021). https://doi.org/10.1016/j.actamat.2020.10.052

Y. Zhang, M. Zecevic, A. Chakraborty, R.J. McCabe, T.J. Nizolek, R.A. Lebensohn, J.S. Carpenter, N. Li, L. Capolungo, Unraveling kinking: a plasticity enhancing failure mode in high strength nano metallic laminates. Acta Mater. **260**, 119342 (2023). https://doi.org/10.1016/j.actamat.2023.119342. https://www.sciencedirect.com/science/article/pii/S1359645423006729

S. Zheng, I.J. Beyerlein, J.S. Carpenter, K. Kang, J. Wang, W. Han, N.A. Mara, High-strength and thermally stable bulk nanolayered composites due to twin-induced interfaces. Nat. Commun. **4**(1), 1–8 (2013). https://doi.org/10.1038/ncomms2651. https://www.nature.com/naturecommunications

C. Zhou, R. Lesar, Dislocation dynamics simulations of plasticity in polycrystalline thin films. Int. J. Plast. **30–31**, 185–201 (2012). https://doi.org/10.1016/j.ijplas.2011.10.001

C. Zhou, S.B. Biner, R. LeSar, Discrete dislocation dynamics simulations of plasticity at small scales. Acta Mater. **58**(5), 1565–1577 (2010). https://doi.org/10.1016/j.actamat.2009.11.001

## Publisher's Note